The Astronomical Journal, 136:118–145, 2008 July doi:10.1088/0004-6256/136/1/118

OPEN CLUSTERS AS GALACTIC DISK TRACERS. I. PROJECT MOTIVATION, CLUSTER MEMBERSHIP, AND BULK THREE-DIMENSIONAL KINEMATICS

Peter M. Frinchaboy[1,2,3] and Steven R. Majewski[2]
Department of Astronomy, University of Virginia, P.O. Box 400325, Charlottesville, VA 22904-4325, USA; pmf@astro.wisc.edu, srm4n@virginia.edu
Received 2007 December 4; accepted 2008 April 8; published 2008 June 3

ABSTRACT

We have begun a survey of the chemical and dynamical properties of the Milky Way disk as traced by open star clusters. In this first contribution, the general goals of our survey are outlined and the strengths and limitations of using star clusters as a Galactic disk tracer sample are discussed. We also present medium-resolution ($R\sim15,0000$) spectroscopy of open cluster stars obtained with the Hydra multi-object spectrographs on the Cerro Tololo Inter-American Observatory 4 m and WIYN 3.5 m telescopes. Here we use these data to determine the radial velocities of 3436 stars in the fields of open clusters within about 3 kpc, with specific attention to stars having proper motions in the *Tycho-2* catalog. Additional radial velocity members (without *Tycho-2* proper motions) that can be used for future studies of these clusters were also identified. The radial velocities, proper motions, and the angular distance of the stars from cluster center are used to derive cluster membership probabilities for stars in each cluster field using a non-parametric approach, and the cluster members so identified are used, in turn, to derive the reliable bulk three-dimensional motion for 66 of 71 targeted open clusters. The high-probability cluster members that we identify help to clarify the color–magnitude sequences for many of the clusters, and are prime targets for future echelle resolution spectroscopy as well as astrometric study with the Space Interferometry Mission (SIM Planetquest).

Key words: Galaxy: fundamental parameters – Galaxy: kinematics and dynamics – Galaxy: structure – open clusters and associations: general

Online-only material: machine-readable and VO tables

1. INTRODUCTION

1.1. Galactic Kinematics Using Open Clusters

Open star clusters have long been exploited as tools for understanding Galactic interstellar dust (e.g., Trumpler 1930a, 1930b; Clayton & Fitzpatrick 1987; Dutra & Bica 2000), the age of the Galactic disk (e.g., Janes & Adler 1982; Twarog & Anthony-Twarog 1989; Phelps et al. 1994; Phelps 1997; Chaboyer et al. 1999; Carraro 1999), the Galactic disk metallicity distribution and age–metallicity relation (e.g., Twarog 1980; Friel & Janes 1993; Friel 1995; Twarog et al. 1997), and, of course, stellar evolution (e.g., Sandage 1957; Cannon 1970; Maeder & Mermilliod 1981; Meynet et al. 1993; Koester & Reimers 1996; Prada Moroni & Straniero 2002). The value of open clusters as tracers of the local Galactic rotation curve has also long been recognized (e.g., Hron 1987; Scott et al. 1995; Glushkova et al. 1998; Loktin & Beshenov 2003; Frinchaboy 2006a). It is in this role as a *dynamical tracer* of the Galactic disk that the present study of open clusters is especially focused.

Star clusters can be effective tracers of the Galactic disk because they offer many advantages over other tracer candidates. First, relative to other tracers, star clusters lend themselves more amenably to age, metallicity, distance, and velocity evaluation. Compared to an isolated field star at the same location in the Galaxy, these quantities are much easier to establish in a star cluster, needing only a properly interpreted color–magnitude diagram (CMD) to establish the first three, while velocities can also be better determined for a star cluster because (1) averaging radial velocity and proper motion data over an ensemble of co-moving stars confers potentially as much as a $\sqrt{N}$ increase in precision for the bulk motion of the ensemble, and (2) better distances allow one to translate proper motions into transverse velocities more accurately. Supplemental knowledge of the age and metallicity of a source confers additional beneficial insights into its proper use as a dynamical tracer with respect to, for example, assumptions about orbit shape and asymmetric drift. Alternatively, one can explore Galactic dynamics as a function of population age and metallicity if all relevant data are available.

On the other hand, there are some complications in the use of open clusters as dynamical tracers. The challenge of proper identification of cluster members can present particular hazards. For example, Frinchaboy (2006b) showed that the UCAC stars used by Dias et al. (2006) to establish the proper motions of at least two particular clusters—Be29 and BH176—in their exhaustive survey of over 400 systems are too bright and cannot be part of these distant systems. Difficulties caused by inaccurate membership censuses are why continued large-scale observational efforts are needed before we can be confident in the use of open clusters as Galactic disk tracers, particularly for more sparse and more distant systems.

To overcome these types of problems, which are typically associated with small number statistics, it is desirable to survey large numbers of potential open cluster members. However, this desire to achieve the largest possible statistical samples often encourages a dangerous reliance on compilations of disparate data. For example, the dynamical study of the Galactic disk using open clusters by (Hron 1987) found that in their compilation of data from the literature ∼50% of the clusters with multiple

[1] Current Position: National Science Foundation Astronomy and Astrophysics Postdoctoral Fellow, University of Wisconsin–Madison, Department of Astronomy, 5534 Sterling Hall, 475 N. Charter Street, Madison, WI 53706, USA.
[2] Visiting Astronomer, Kitt Peak National Observatory and Cerro Tololo Inter-American Observatory, National Optical Astronomy Observatory, which is operated by the Association of Universities for Research in Astronomy, Inc. (AURA) under cooperative agreement with the National Science Foundation.
[3] Any opinions, findings, and conclusions or recommendations expressed in this material are those of the author and do not necessarily reflect the views of the National Science Foundation (NSF).

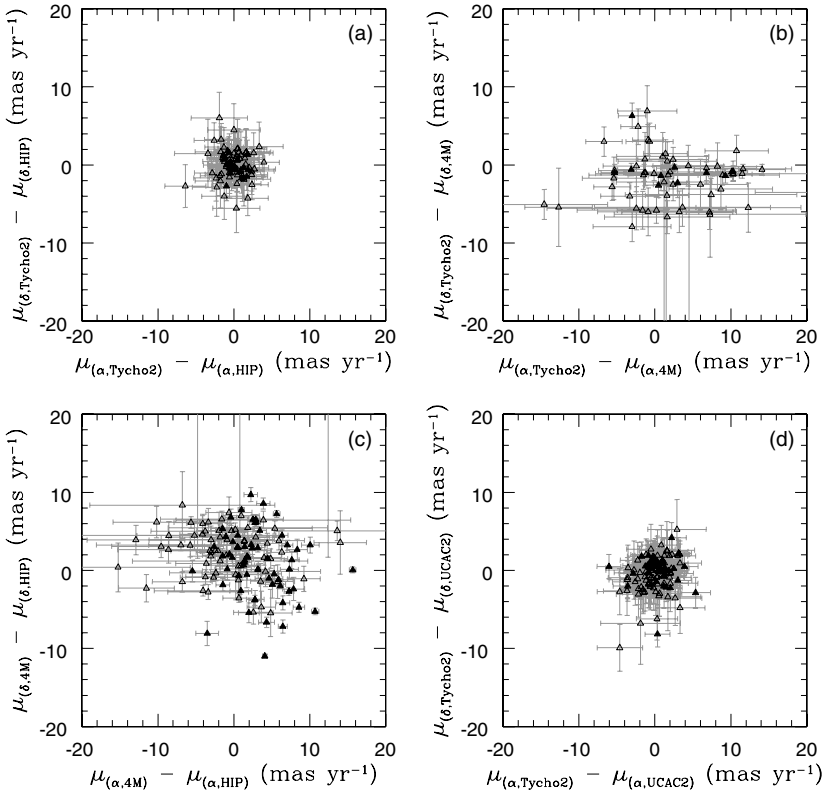

Figure 1. Comparison of proper motions $\Delta\mu_{\alpha\cos\delta}$ and $\Delta\mu_{\delta}$ derived from the *Hipparcos* (Baumgardt et al. 2000), *Tycho-2* (Dias et al. 2001, 2002a), 4M (Glushkova et al. 1996) and the new UCAC-2 (Dias et al. 2006) surveys. (a) *Hipparcos* vs. *Tycho-2*. (b) 4M vs. *Tycho-2*. (c) *Hipparcos* vs. 4M. (d) UCAC-2 vs. *Tycho-2*. Error bars are the quadrature combination of the uncertainties in the two surveys. Filled triangles denote clusters with best errors ($\Delta\epsilon_{\mu_\alpha}$ and $\Delta\epsilon_{\mu_\delta} <$ 2.0 mas yr^{-1}).

distance measurements had differences greater than 1 magnitude in determined distance modulus and ∼50% of the clusters also had poor RV qualities.[4]

To help overcome both the membership and homogeneity problems that are often a hindrance to the use of open clusters as tracers of the Galactic disk, we present a new survey of open clusters that will not only take advantage of quality radial velocities to help discriminate cluster members, but also rely on one source of data as much as possible for each independent cluster parameter (e.g., all photometry from one source, all RVs and derived in a uniform manner, all proper motions coming from one catalog, etc). A central objective of this study is the use of these clusters to derive global dynamical properties of the Milky Way disk, with a particular emphasis on the derivation of the full space velocities for the target clusters. In keeping with our philosophy of uniformity of data, and because large numbers of proper motions at present must come from all-sky astrometric surveys, we first investigate the main proper motion catalogs available for investigations of open cluster kinematics, from which we might draw an initial target sample.

1.2. All-Sky Proper Motion Surveys: Hipparcos, Tycho-2, UCAC-2, and the 4M

A key advance that has propelled a resurgence in the use of open clusters as disk dynamical tracers is the compilation of all-sky proper motion surveys. There have been four surveys to determine bulk Galactic cluster kinematics by averaging the proper motions of presumed cluster stars based on data from the *Hipparcos* (Baumgardt et al. 2000), *Tycho-2* (Dias et al. 2001, 2002a), Four Million Star (4M) (Glushkova et al. 1996), and recently the UCAC-2 (Dias et al. 2006) catalogs. The European Space Agency (ESA) *Hipparcos* mission has provided critical astrometry for two of these proper motion databases via each of *Hipparcos'* primary data products: (1) the *Hipparcos* catalog of ∼118, 000 stars ($V \leqslant 11$) with proper motion uncertainties of 1–2 mas yr^{-1} and (2) the *Tycho-2* catalog of 2.5 million stars ($V \leqslant 13.5$) with proper motion uncertainties of 1–3 mas yr^{-1}. The UCAC-2 catalog of 48 million stars is based on *Tycho-2* and fainter, ground-based observations (to $R = 16$) and has proper motion uncertainties of 1–7 mas yr^{-1}. The 4M catalog (Volchkov et al. 1992) was compiled from the Astrographic Catalog and the *Hubble Space Telescope* guide star catalog (GSC) reduced to the older system of the PPM (Röser & Bastian 1991; Bastian et al. 1993; Röser et al. 1994) survey, with proper motion uncertainties of ∼10 mas yr^{-1}.

Proper motions for hundreds of open clusters have been published using these catalogs. However, a comparison of the derived motions for the clusters in common between surveys reveals substantial discrepancies, as shown in Figure 1, where a cluster-by-cluster comparison of the proper motion differences is illustrated, namely for (a) *Tycho-2* versus *Hipparcos*, (b) *Tycho-2* versus 4M, (c) 4M versus *Hipparcos*, and (d) *Tycho-2* versus UCAC-2. As may be seen, differences in derived proper motions typically exceed the quoted uncertainties claimed by each survey. The best correlation of derived proper motions is between surveys using the *Tycho-2* and *Hipparcos* astrometry; remaining differences in derived mean cluster proper motions between these surveys must therefore be due to differences in

[4] It is worth pointing out that this is a common problem with other types of Galactic rotation tracers that have been adopted in the past, not just open clusters.

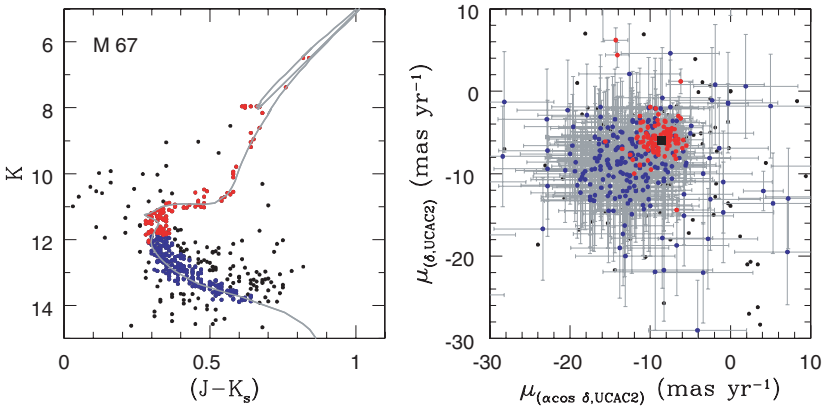

Figure 2. (a) 2MASS CMD of all UCAC-2 stars within the 25′ radius of M67 with Salasnich et al. (2000) 2MASS isochrone overplotted. Red points denote stars brighter than magnitude = 13.0 in the UCAC system (approximately equal to the Cousins *R* band), that are selected to be along the cluster's stellar sequence in the CMD while blue points denote stars fainter than 13.0 that lie the cluster's main sequence. (b) Comparison of proper motions μ_α and μ_δ derived for M67 stars from the UCAC-2 survey. The red and blue points denote the same stars as in (a). One can see that by adding the fainter UCAC-2 data, and thereby changing which survey the proper motion data are primarily derived from, one can actually change the derived bulk proper motion by almost 2 mas yr^{-1} in each direction. The black square denotes the measured bulk proper motion from the Dias et al. (2001) survey.

the adopted samples of presumed cluster members because the actual proper motions, at least for $V \lesssim 11$, are the same (i.e. *Hipparcos*-based), while the *Tycho-2* astrometry used at fainter magnitudes is on the *Hipparcos* reference system (which means that the system is referenced to background, extra-galactic sources of the International Celestial Reference System). Of course, with its bright magnitude limit, *Hipparcos* can usually provide useful astrometry for only a small number of stars per cluster (typically less than four). With only a few stars per cluster, a *Hipparcos*-based survey is far more susceptible to small number statistics as well as the misidentification of true cluster members against the large number of fore/background stars of the Galactic disk.

1.3. A Closer Look at the UCAC-2 and 4M Catalogs

Clearly *Tycho-2* and *Hipparcos*, which are currently the most accurate all-sky astrometric surveys, must be considered primary and important sources of proper motion data for our survey. On the other hand, deeper catalogs can provide more cluster members, but typically with worse precision. Thus, it is not immediately obvious that adding additional data from the deeper proper motion catalogs improves or degrades those from *Tycho-2* and *Hipparcos* alone. A reasonable correlation of derived cluster motions is found when either the *Tycho-2* and UCAC-2 catalog data are used with a $V \leqslant 13$ limit, but this is because UCAC-2 adopts *Tycho-2* proper motions for stars brighter than about $V = 13$ (Zacharias et al. 2004). On the other hand, it is clear that there are greater deviations in derived proper motions when we incorporate the fainter stars from UCAC-2. Apart from not knowing whether these differences reflect systematic problems in the fainter UCAC catalog (which allows probing of proper motions with stars to $V = 16$) or small number statistics in the brighter surveys, some additional concerns about UCAC beyond those suggested by Figure 1 have led us not to adopt this dataset for our own work.

For example, as recently pointed out in Balaguer-Núñez et al. (2007), the UCAC-2 proper motions may have systematic trends with magnitude due to the compiled nature of the UCAC-2 survey (i.e., ground-based proper motions are added to *Tycho-2* data). This concern is usefully illustrated by looking at the cluster M67 (NGC 2682). In Figure 2(a), we show the Two Micron All Sky Survey (2MASS; Skrutskie et al. 2006) CMD for the M67 field plotting only the most probable members based on CMD location. We split the CMD (red: UCAC mag < 13.0, blue: UCAC mag $\geqslant 13.0$) at a magnitude that represents approximately the transition within the catalog from *Tycho-2* to ground-based observations. Substantial proper motion shifts are apparent between the bright and faint samples (Figure 2(b)), and this suggests significant systematic zero-point offsets within the UCAC-2 database.

The 4M catalog, as well, appears to have systematic proper motion errors. The 4M is not tied to the *Hipparcos* system, but rather to the PPM (Gulyaev & Nesterov 1992). Glushkova et al. (1996, 1998) have used the 4M catalog to determine the proper motions of about 200 open clusters. Dias et al. (2001) compared their *Tycho-2* open cluster proper motions to both those based on *Hipparcos* (Baumgardt et al. 2000) and the Glushkova et al. 4M work and found that the 4M motions were systematically offset from those in the *Hipparcos* system by ∼5 mas yr^{-1} in both $\mu_\alpha \cos\delta$ and μ_δ, an amount that was larger than expected given the quoted errors of both the surveys. While these differences likely reflect both differences in membership as well as astrometric accuracy, this comparison suggests that the deeper proper motions are not necessarily providing better overall accuracy in the open cluster bulk motions, and recommends a strategy based on quality over quantity of cluster star motions.

Therefore, because of uncertainty over the reliability of the UCAC-2 and 4M surveys and our desire to adhere to a "quality over quantity" policy, we have elected to focus on deriving bulk motions using astrometry from the *Tycho-2* catalog, but with a dedication to ensuring that we derive a trustworthy membership of the smaller number of available cluster stars available in this shallower database.

1.4. A New Galactic Tracer Survey

The mass and mass distribution of the Galactic disk has been a matter of debate for over a century, and will likely remain so until extremely precise proper motions and trigonometric parallaxes can be obtained for numerous disk tracers, most likely through future space-based studies like the National Aeronautics and Space Administration's (NASA) *Space Interferometry Mission* (*SIM PlanetQuest*) and the ESA's *Gaia* satellites. The new project presented here represents both a preparatory effort in

this space-based direction as well as a standalone dynamical study in its own rite. Our goal is to establish a well-constructed, well-studied, baseline tracer population—open clusters—that can not only (1) serve as input targets for Galactic dynamics studies with *SIM PlanetQuest* (specifically, for the *SIM* Key Project *Taking Measure of the Milky Way*, for which SRM is the principal investigator and which has provided support for this project), but which (2) can also be immediately exploited for understanding Galactic dynamics with existing astrometric data.

As mentioned above, the inability to establish a uniform, unbiased tracer sample has been one of the key weaknesses of previous Galactic dynamical surveys (e.g., Fich et al. 1989). To provide a homogeneous set of tracers, we have undertaken a spectroscopic survey to obtain precision RVs of open cluster fields. These RVs will establish cluster membership for individual stars that not only provides a very precise mean RV of each cluster, but, in identifying cluster members having accurate astrometry, can be used to define the bulk cluster proper motion. The combination of the newly found, very precise mean RV of each cluster with its derived bulk proper motion and distance will allow us to determine the space velocities of these clusters. With a large number of cluster space velocities, the rotation curve of the Galactic disk can be constrained over the R_{gc} range of the sample. Alternatively, through the adoption of an assumed rotation curve (i.e., Galactic potential), the orbital properties of individual clusters can be determined.

Because we are interested in obtaining results before *SIM PlanetQuest* and *Gaia* are in service, our RV study will focus on clusters already having available, uniform, and reliable proper motions. As described in Section 1.4, we have elected to focus on the all-sky *Tycho-2* proper motion catalog, which provides useful astrometry for typically 50–200 stars per cluster field ($\leqslant$0.75 deg^2). While selection of *Tycho-2* as our source of proper motions limits the depth and thereby the cluster distance that can be explored, it is in keeping with our philosophy of quality over quantity for the astrometric data. The selected proper motion stars for a given cluster field can usually be investigated spectroscopically with a single pointing of the NOAO Hydra multi-fiber spectrographs on the CTIO 4 m and WIYN[5] 3.5 m telescopes, and the radial velocities derived from these spectroscopic data are the primary results presented here. Our campaign of multi-fiber spectroscopy allows us to check virtually every star in a cluster field having a *Tycho-2* proper motion, and leaves additional fibers to (1) expand the RV membership census to fainter stars in anticipation of the future astrometric surveys (e.g., *SIM* and *Gaia*), and (2) improve age-dating of the clusters through CMD-isochrone fitting to established member stars. The current study of clusters provides a large uniform database for further open cluster research, as a supplement to the Dias et al. (2002b) and WEBDA (Mermilliod 1995) databases.

The new RVs immediately improve all previous proper motion work on our targeted clusters because of the clarity they bring regarding cluster membership. The improved RVs and proper motions, when combined with new distances we shall derive elsewhere (Paper II), will provide much more reliable space motions of numerous open clusters over a large R_{gc} range; these space velocities will be at a precision sufficient to make tangible improvements in the determination of the nearby Galactic rotation curve and, in turn, the mass distribution of the Galactic disk. With uncertainties of order $\sim$1.2 km s^{-1}, the data here yield the best-derived bulk RVs thus far for most of the chosen clusters, This precision is comparable to the uncertainties in transverse velocity that SIM and *Gaia* will measure for these clusters, and represent a significant improvement over many previous RV surveys of open clusters, which have typical uncertainties of order $\sim$15 km s^{-1} (Scott et al. 1995). Our results are more comparable to the RV precisions being obtained for open cluster stars in studies using CORAVEL (e.g., Mermilliod & Mayor 1989, 1990), for example.

Following the work in this paper (Paper I), we will provide uniformly-determined distances and ages derived from isochrone-fitting to 2MASS photometry of these clusters, aided by the cluster membership data derived here (Paper II). With newly-derived kinematics and distances in hand from Papers I and II, we will then use the cluster sample to explore not only the orbital characteristics of the individual clusters (Paper III), but the global properties of the Galactic disk (Paper IV), including: (1) the local Galactic rotation curve and velocity field near the Sun, (2) the kinematics of the disk across the frontier separating $R < R_0$ and $R > R_0$, and (3) the validity of the assumption of Galactic dynamical symmetry (e.g., north versus south, Galactic quadrants I/II versus IV/III).

In Section 6 and Table 12 of this paper we present the derived 3D space motions of the clusters that enable these future contributions. In the preceding sections of this paper we explain how we selected our target clusters (Sections 2.1 and 4) and which stars within each cluster field to probe (Section 2.2), the spectroscopic observations and the derivation of radial velocities (Section 3), and the means by which membership within each cluster is established (Section 5).

2. SOURCE SELECTION

2.1. Cluster Sample Selection

Our selection of specific open clusters starts with the 205 clusters explored in the Dias et al. (2001, 2002a) catalogs, which derive cluster membership using the statistical method of Sanders (1977). We also adopt the following criteria: (1) the clusters must have at least ten stars with *Tycho-2* proper motions in the fields selected by Dias et al. (2001, 2002a), and (2) the cluster diameters cannot be much larger than the Hydra field of view (40′: CTIO; 60′: WIYN) so that the cluster can be sampled with a significant number of fibers. In addition, to obtain the greatest leverage on the local Galactic rotation curve the selected clusters span a wide area over the Galactic X_{gc}–Y_{gc} plane and reach to a heliocentric distance of $\geqslant$2.5 kpc. Neither age, distance from the Galactic plane, nor metallicity was considered as a selection criterion.

Table 1 shows the basic cluster parameters of our sample with data taken from the Dias et al. (2002b) catalog, including coordinates of right ascension and declination (Columns 2 and 3) and Galactic longitude and latitude (Columns 4 and 5), heliocentric distance (Column 6), log(age/years) and visual diameter of the cluster in arcminutes (Columns 7 and 8), and the observing run on which the cluster was observed (see below and Table 3 for definitions). The Galactic distribution of our final cluster sample of 71 clusters is shown in Figure 3. The smaller number of clusters we have sampled in the l = 0–180°half of the Galaxy is result of a smaller amount of observing time obtained for the WIYN observations; however, future work in the

[5] The WIYN Observatory is a joint facility of the University of Wisconsin–Madison, Indiana University, Yale University, and the National Optical Astronomy Observatories.

Table 1
Dias et al. (2002b) Target Cluster Properties

Cluster	α_{2000}	δ_{2000}	l (°)	b (°)	d (pc)	log(age) (yr)	Diameter (′)	Run
NGC 129	00:30:00	+60:13:06	120.2701	1.4566	1625	7.886	19	5
NGC 381	01:08:19	+61:35:00	294.3672	0.1870	1148	8.505	6	5
NGC 457	01:19:35	+58:17:12	303.2056	0.2577	2429	7.324	20	5
NGC 884	02:22:18	+57:08:12	141.2419	−10.6452	2345	7.032	18	5
NGC 957	02:33:21	+57:33:36	124.6487	−13.4947	1815	7.042	10	5
NGC 1513	04:09:57	+49:30:54	152.5898	−1.5743	1320	8.110	10	5
NGC 1528	04:15:23	+51:12:54	152.0568	0.2577	776	8.568	16	5
NGC 1662	04:48:27	+10:56:12	187.6949	−21.1142	437	8.625	20	4
Stock 8	05:27:36	+34:25:00	173.3194	−0.2808	1821	7.056	14	5
NGC 1960	05:36:18	+34:08:24	174.5344	1.0720	1318	7.468	10	5
NGC 2099	05:52:18	+32:33:12	177.6353	3.0913	1383	8.540	14	5
Kharchenko 1	06:08:48	+24:19:54	186.5813	2.1705	2520	8.000	7	5
NGC 2215	06:20:49	−07:17:00	215.9932	−10.1024	1293	8.369	7	2
NGC 2264	06:40:58	+09:53:42	202.9357	2.1957	667	6.954	39	1,2
NGC 2301	06:51:45	+00:27:36	212.5580	0.2791	872	8.216	14	1
NGC 2323	07:02:42	−08:23:00	221.6722	−1.3311	929	8.096	14	1
NGC 2354	07:14:10	−25:41:24	238.3683	−6.7918	4085	8.126	18	2
NGC 2353	07:14:30	−10:16:00	224.6853	0.3841	1119	7.974	18	2
NGC 2423	07:37:06	−13:52:18	230.4835	3.5368	766	8.867	12	2
NGC 2437	07:41:46	−14:48:36	231.8575	4.0644	1375	8.390	20	2
NGC 2447	07:44:30	−23:51:24	240.0386	0.1345	1037	8.588	10	2
NGC 2482	07:55:12	−24:15:30	241.6257	2.0345	1343	8.604	10	1
NGC 2516	07:58:04	−60:45:12	273.8157	−15.8558	409	8.052	30	2
NGC 2527	08:04:58	−28:08:48	246.0873	1.8549	601	8.649	10	2
NGC 2547	08:10:09	−49:12:54	264.4648	−8.5974	455	7.557	25	2
NGC 2539	08:10:37	−12:49:06	233.7053	11.1115	1363	8.570	9	2
NGC 2546	08:12:15	−37:35:42	254.8551	−1.9859	919	7.874	70	1
NGC 2548	08:13:43	−05:45:00	227.8724	15.3928	769	8.557	30	1
NGC 2567	08:18:32	−30:38:24	249.7950	2.9609	1677	8.469	7	2
NGC 2579	08:20:52	−36:13:00	254.6741	0.2126	1033	7.610	7	2
NGC 2670	08:45:30	−48:48:00	262.1476	0.7868	1188	7.690	7	2
NGC 2669	08:46:22	−52:56:54	267.4854	−3.6250	1046	7.927	20	2
Trumpler 10	08:47:54	−42:27:00	262.7906	0.6740	424	7.542	29	1
NGC 2682	08:51:18	+11:48:00	122.9232	−27.0400	908	9.409	25	1
Collinder 205	09:00:32	−48:59:00	269.2091	−1.8434	1853	7.200	5	2
IC 2488	09:27:38	−57:00:00	277.8298	−4.4192	1134	8.113	18	1
NGC 2925	09:33:11	−53:23:54	274.6855	1.7570	774	7.850	10	1
NGC 3680	11:25:38	−43:14:36	124.9390	−1.2226	938	9.077	5	2
Collinder 258	12:27:10	−60:46:00	299.9710	1.9654	1184	8.032	5	1,2
NGC 5281	13:46:35	−62:55:00	309.0102	−2.4915	1108	7.146	7	2
NGC 5316	13:53:57	−61:52:06	311.6017	2.1144	1215	8.202	14	2
Lynga 1	14:00:02	−62:09:00	310.8493	−0.3373	2283	8.007	3	2
NGC 5460	14:07:27	−48:20:36	316.3148	5.6067	678	8.207	35	2
Lynga 2	14:24:35	−61:20:00	313.8642	−0.4544	1000	8.122	10	1
NGC 5617	14:29:44	−60:42:42	317.5264	2.0851	1533	7.915	10	2
NGC 5662	14:35:37	−56:37:06	319.5288	4.5444	666	7.968	29	1
NGC 5822	15:04:21	−54:23:48	324.3610	1.7201	917	8.821	35	2
NGC 5823	15:05:30	−55:36:12	343.8165	19.8092	1192	8.900	12	2
NGC 6025	16:03:17	−60:25:54	329.7454	−2.2048	756	7.889	14	1
NGC 6031	16:07:35	−54:00:54	327.7257	−5.4256	1823	8.069	3	2
NGC 6067	16:13:11	−54:13:06	127.7404	2.0870	1417	8.076	14	2
Harvard 10	16:18:48	−54:56:00	329.8356	−3.2844	1312	8.340	25	2
NGC 6124	16:25:20	−40:39:12	332.9179	−3.1668	512	8.147	39	1
NGC 6134	16:27:46	−49:09:06	335.2223	−1.4272	913	8.968	6	2
Ruprecht 119	16:28:15	−51:30:00	333.2758	−1.8794	956	6.853	8	1
NGC 6167	16:34:34	−49:46:18	338.4047	1.2106	1108	7.887	7	1
NGC 6250	16:57:56	−45:56:12	341.9974	−1.5166	865	7.415	10	4
NGC 6281	17:04:41	−37:59:06	345.2791	−3.0564	479	8.497	8	2
IC 4651	17:24:49	−49:56:00	340.0881	−7.9068	888	9.057	10	1
NGC 6405	17:40:20	−32:15:12	356.9316	−1.5491	487	7.974	20	2
NGC 6416	17:44:19	−32:21:42	357.9402	−1.6054	741	8.087	14	2
NCG 6603	18:18:26	−18:24:24	15.8996	0.3505	3600	8.300	6	2,3
IC 4756	18:39:00	+05:27:00	36.3807	5.2422	484	8.699	39	4
NGC 6705	18:51:05	−06:16:12	15.3951	−9.5927	1877	8.302	13	4
NGC 6811	19:37:17	+46:23:18	73.9778	8.4808	1215	8.799	14	5
NGC 6866	20:03:55	+44:09:30	60.3897	−6.0501	1450	8.576	14	5

Table 1
(Continued)

Cluster	α_{2000}	δ_{2000}	l (°)	b (°)	d (pc)	log(age) (yr)	Diameter (′)	Run
NGC 6885	20:11:58	+26:29:00	66.1352	−6.3113	597	9.160	10	4
Berkeley 86	20:20:24	+38:42:00	76.6667	1.2725	1112	7.116	6	5
Platais 1	21:30:02	+48:58:36	92.5613	−1.6461	1268	8.244	10	5
NGC 7209	22:05:07	+46:29:00	102.7010	0.7820	1168	8.617	14	5
NGC 7654	23:24:48	+61:35:36	117.2878	10.8044	1421	7.764	15	5

Notes.
[a] Run 1: 2002 March (CTIO); Run 2: 2003 March (CTIO); Run 3: 2003 June (CTIO); Run 4: 2003 August (CTIO); Run 5: 2003 September (WIYN).

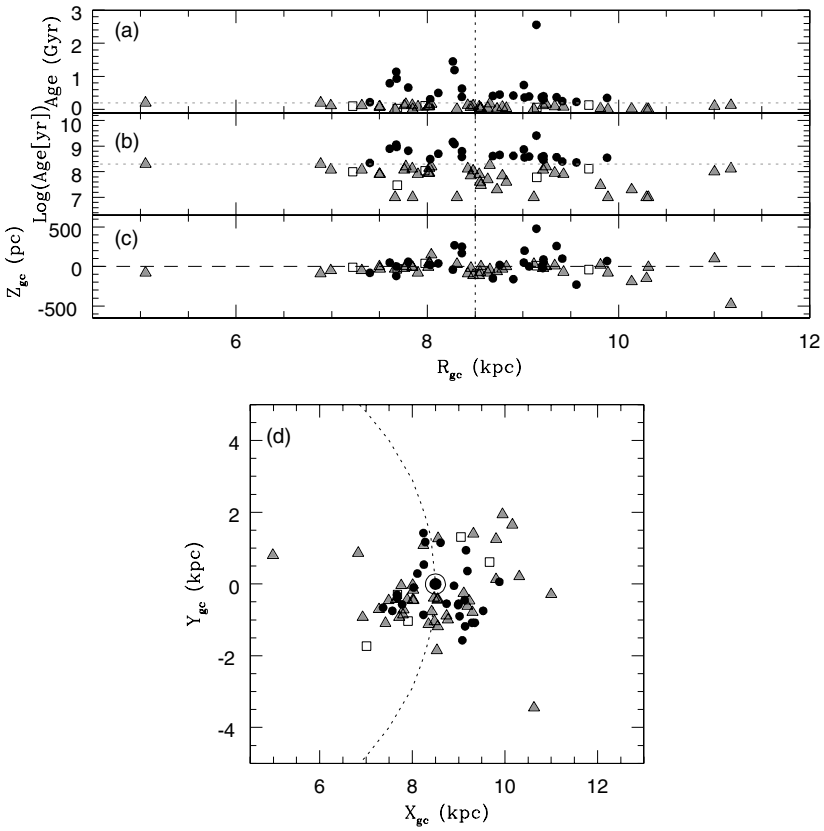

Figure 3. Properties of the open cluster sample. (a) Plot of cluster age vs. R_{gc}. One can see that most clusters are less than 200 Myr old (gray triangles) though a number of old clusters are present in the sample (black circles). Open squares denote the clusters Collinder 258, Lynga 1, NGC 1513, NGC 6250, and NGC 7654 (see Sections 6.1 and 6.2.3), which we excluded from our sample because our results for these clusters are uncertain. (b) The same as (a), but showing a smaller age range. (c) Distribution of Z_{gc} (height above/below the Galactic plane) vs. R_{gc}. (d) X_{gc}, Y_{gc} distribution of clusters in this study.

research program will aim to remedy this deficiency. Figure 3 also shows the distribution of the selected cluster ages and distances from the Galactic midplane as a function of their Galactic radius (assuming the Sun is at 8.5 kpc). More than half of our final sample have ages less than 200 Myr but older than 10 Myr (Table 1). The large number of relatively young clusters is important for kinematical studies of the Galactic disk because, in general, open clusters should develop increasing deviations from "normal" disk rotation due to the scattering by molecular clouds over time (Spitzer & Schwarzschild 1951, 1953); however, clusters that are *too* young may still reflect the specific dynamical environment of their birth and may not yet have circular orbits (Lynga & Palous 1987). Figure 3(c) shows that all clusters in our sample are within 500 pc of the Galactic plane, and most are within 200 pc. This supports the notion that most clusters in our sample are likely to be "well behaved" in the sense that they have not been scattered far from the Galactic midplane and therefore are likely to still be on near-circular orbits (of course, we will revisit this question when we examine cluster orbits in detail, in a future contribution).

Less than 25% of our clusters have estimated metallicities ([Fe/H]), so we have little leverage on this aspect of our sample; however, we hope to derive metallicity estimates for some of our clusters in the future, using not only improved isochrone fits to CMDs aided with our membership data, but the spectra themselves.

2.2. Stellar Selection Within Each Cluster

Given that bulk 3D motions are our primary goal, the first stellar targets within each cluster selected for observation were those *Hipparcos* and *Tycho-2* stars used in the Dias et al. (2001, 2002a) survey for the clusters. Because constraints on fiber optic placement with the Hydra instrument (i.e., two fibers cannot be closer than 25″ in the Hydra setup) mean that in some cases not all desired stars can be observed in a cluster field, we must prioritize stars within a fiber setup. For this reason,

stars were ranked in priority order based on the Dias et al. (2001, 2002a) derived membership probabilities, from highest to lowest probability. Dias et al. (2001, 2002a) derived these probabilities based on the proper motions using the method of Sanders (1977).

Next, additional *Tycho-2* stars available in the Hydra field of view, but not used in the Dias et al. (2001, 2002a) study (because they lie beyond the cluster radius studied by these authors) were added as the next priority to the target list. For the WIYN/Hydra runs, no targets beyond the *Tycho-2* stars needed to be selected because the combination of a smaller number of available Hydra fibers (90 versus 132 for CTIO/Hydra) and larger field of view (60′versus 40′for CTIO/Hydra) typically meant that nearly all target fibers were filled with *Tycho-2* stars.

For the CTIO runs and for fields having less than 50 stars with available *Tycho-2* proper motion data, we selected at lowest priority two additional sets of stars; first, stars between $V =$ 13–15 magnitude from the USNO-B1.0 catalog from within the cluster radius (with that value taken from the Dias et al. 2002b catalog), with the goal of searching for additional cluster members fainter than the $V \sim 13.5$ magnitude limit of the *Tycho-2* survey, and second, we allowed unused "field orientation probe stars" (FOPS; USNO B1.0 stars with $12 < R_2 < 13$) to be added to the bottom of the target priority list. At either WIYN or CTIO, fibers that were not assigned to targets were used for sky observations, with at least six (WIYN) or ten (CTIO) fibers positioned on random sky for sky subtraction of the stellar spectra.

3. SPECTROSCOPIC SURVEY DATA

3.1. Spectroscopic Observations

We have collected homogeneous spectroscopic observations for 71 open clusters using the HYDRA multi-fiber spectrographs on the Blanco 4 m telescope at Cerro Tololo Inter-American Observatory (CTIO) and the 3.5 m WIYN telescope at Kitt Peak National Observatory (KPNO). This project was conducted using publicly competed NOAO time and was granted long-term status,[6] which permitted observations in the semesters 2002A–2004A over a total of 14 awarded CTIO 4 m and six WIYN 3.5 m nights. The data for the clusters listed in Table 1 were obtained the nights of UT 2002 March 8–12 ("Run 1"), 2003 March 16–21 ("Run 2"), 2003 July 20–23 ("Run 3"), and 2003 August 2–8 ("Run 4") from CTIO. For more efficient observing, some cluster observations scheduled for two August 2003 CTIO nights were interspersed with other targets for two other observing projects awarded telescope time over the course of eleven CTIO/Hydra nights in 2003 July and August (Runs 3 and 4). The WIYN data were observed on the nights of 2003 September 14–18 ("Run 5").

The CTIO observations made use of 132 Hydra fibers that are simultaneously dispersed onto a 2048×4096 pixel, SITe400mm CCD using the 380 grating with 1200 lines mm^{-1}, and with the fiber ends viewed by the spectrograph through the 100 μm slit plate to improve the resolution to a dispersion of 0.68 Å per resolution element ($R \sim 15,000$). The spectral range covered was 7740–8740 Å. Data obtained at WIYN dispersed the 90 Hydra fibers dispersed onto a 2048×2048 pixel CCD in the Red Bench Camera using the echelle (316@63.4) grating in sixth order; this yielded a dispersion of 0.82 Å per resolution element ($R \sim 13,000$) which was centered on the 8220–8800 Å spectral range. Typical signal-to-noise ratios (S/N) of 10 or better were obtained; all cluster stars presented have at least S/N $\geqslant 5$. To aid the RV calibration, multiple RV standards were observed on each run, where each "observation" of an RV standard entails sending the light of the calibrator down 2–12 different fibers, yielding many dozen individual spectra of each RV standard. We present here the results from analysis of spectra for 3436 individual stars out of 3537 with sufficient S/N observed in the fields of 71 open clusters.[7]

3.2. Data Reduction

Preliminary processing of the two-dimensional data was undertaken using standard IRAF[8] techniques as described in the IRAF `ccdproc` documentation. After completing the CCD bias subtraction, overscan correction and trimming, the two-dimensional images were corrected for pixel-to-pixel sensitivity variations and chip cosmetics by applying "milky flats" according to the prescription outlined in the CTIO Hydra manual by N. Suntzeff.[9]

After basic processing the data were run through the IRAF routine `dohydra`. One-dimensional spectra for each star were extracted from the two-dimensional CCD images and wavelength calibrated with respect to a comparison lamp spectrum. Exposures of the PENRAY (CTIO; He, Ne, Ar, and Xe) or CuAr (WIYN) lamps were taken at each Hydra pointing through all fibers to provide comparison spectra yielding at least 11 prominent emission lines roughly evenly distributed over the observed wavelength range. These comparison spectra provide a wavelength solution (i.e., pixel to wavelength conversion) for each extracted object spectrum.

3.3. Stellar Radial Velocities: Standard Stars

All radial velocities were derived using IRAF's `fxcor` package, which we used first to determine RVs for the standard stars. Radial velocity standard stars are used to check for systematics in the data, to determine the measured RV precision, and to calibrate the zero-point of the velocity scale. The reduction to radial velocities employed essentially the classical cross-correlation methodology of Tonry & Davis (1979). The template star input to the correlator is prepared from a high-S/N standard star spectrum from which the stellar continuum is fitted and subtracted. The resulting spectrum is high- and low-pass Fourier-filtered to remove both high-frequency noise (e.g., cosmic rays) and the low-frequency variation cause by difference in instrument throughput.

We first measured the RVs of standard stars by cross-correlating each Fourier-filtered standard star spectrum against every other standard star spectrum from its corresponding observing run over the restricted wavelength range of 8220–8680 Å, which avoided possible contamination from nearby atmospheric lines. The resulting RVs from different cross-correlations for each individual standard star spectrum were averaged and the standard deviations measured; the results are presented in Table 2. The average velocity standard deviation for the individual Hydra standard star spectra is $\sigma_v \lesssim 2$ km s^{-1} for spectra with S/N $\geqslant 20$.

[6] This project was selected as an NOAO Ph.D. thesis project for PMF.

[7] Of the 3537 stars observed with S/N > 5, 101 were peculiar stars (e.g., carbon stars, Be stars, young emission-line stars) that are excluded from the RV analysis using "normal star" cross-correlation templates discussed here.

[8] IRAF is distributed by the National Optical Astronomy Observatory, which is operated by the Association of Universities for Research in Astronomy, Inc., under cooperative agreement with the National Science Foundation.

[9] http://www.ctio.noao.edu/spectrographs/hydra/hydra-nickmanual.html.

Table 2
RV Standard Observations

UT date	Star	Spec. type	Frame #	Fiber	TDR	V_r (km s^{-1})	ϵ_V (km s^{-1})	Avg. (km s^{-1})	$\epsilon_{V,\mathrm{avg}}$ (km s^{-1})	IAU (km s^{-1})
					2002 March					
2002 Mar 11	HD 12605	A0 V	0028	005	34.88	−19.97	2.18			
2002 Mar 11	HD 12605	A0 V	0028	029	35.35	−21.50	2.17			
2002 Mar 11	HD 12605	A0 V	0028	032	37.84	−20.45	1.86			
2002 Mar 11	HD 12605	A0 V	0028	035	37.25	−20.31	2.02			
2002 Mar 11	HD 12605	A0 V	0028	082	32.95	−20.98	1.76			
2002 Mar 11	HD 12605	A0 V	0028	111	29.99	−19.91	1.87			
2002 Mar 11	HD 12605	A0 V	0028	119	31.73	−20.76	1.58			
2002 Mar 11	HD 12605	A0 V	0028	124	28.99	−21.13	1.74			
2002 Mar 11	HD 12605	A0 V	0028	126	33.70	−21.71	1.91	−20.75	0.64	-18.5 ± 0.4
2002 Mar 11	HD 157457	G8 III	0029	010	59.12	+18.86	1.74			

Notes.
Stars HR 7773 and HR 675 are not IAU RV standards (see Section 3.3).
[a] Due to poor S/N this star was not used as a cross-corelation template.
(This table is available in its entirety in machine-readable and Virtual Observatory (VO) forms in the online journal. A portion is shown here for guidance regarding its form and content.)

Table 3
Calibration of RV Errors

Run dates	Run#	Star colors	Degrees of freedom	χ^2_{50}	α	Telescope
2002 Mar 10–13	1	Red	24	23.337	35.19	CTIO 4 m
2003 Mar 16–21	2	Red	22	21.337	27.69	CTIO 4 m
2003 Jul 19–22	3	Red	41	40.334	50.24	CTIO 4 m
2003 Aug 01–07	4	Red	72	71.333	33.59	CTIO 4 m
2003 Aug 01–07	4	Blue[a]	9	8.343	84.87	CTIO 4 m
2003 Sep 14–17	5	Red	6	5.3481	53.22	WIYN 3.5 m
2003 Sep 14–17	5	Blue	6	5.3481	41.14	WIYN 3.5 m

Note. [a] These data were used as "blue" cross-correlation templates for all CTIO runs.

We determined the level of the random and any unknown systematic RV errors from a prescription described in Vogt et al. (1995), which is based on the analysis of repeatedly observed stars (Table 2). In this case these stars were typically observed through different Hydra fibers. The Tonry–Davis Ratio (TDR; Tonry & Davis 1979) for each spectrum is measured using `fxcor`. Since the TDR scales approximately with S/N we can, following the method described in Vogt et al. (1995), determine approximate 1σ errors in the RVs corresponding to a given TDR as

$$\text{error } V_r = \frac{\alpha}{(1 + \text{TDR})}. \quad (1)$$

The parameter α is a constant calibrated by the standard star data using the following formula, which is predicated on the assumption that the TDR is a good measure of the relative S/N, and where autocorrelations are not included:

$$\alpha^2 = \frac{\sum_i \sum_j (1 + \text{TDR}_{i,j})^2 (V_{r,i,j} - \langle V_{r,j} \rangle)^2}{\chi^2_{50,n}} \quad (2)$$

where $V_{r,i,j}$ is the ith observation of the jth standard star, and $\langle V_{r,j} \rangle$ is the mean RV of the jth standard star. We obtained the values of χ^2_{50} for our sample's number of degrees of freedom, where $\chi^2_{50,n}$ is the critical value of the χ^2 distribution at the 50% confidence level multiplied by n degrees of freedom, as described fully in Vogt et al. (1995).

Since our target stars were selected based on proper motion criteria, they span a wide range of spectral types, including anything from hot O and Be stars to cool carbon stars. As a result, we observed a range of RV standard star templates. However, due to the lack of International Astronomical Union (IAU) RV standards hotter than spectral type A0, we used B and A stars from Fekel (1999) to provide RV standards for our hot star spectra. For a better match in the spectral types between targets and cross-correlation templates, we divided the observed standard stars into "red" or "blue" subsamples for our cross-correlation templates. Stars were considered "red" stars if the Ca II infrared triplet (8498 Å, 8542 Å, and 8662 Å) was present in the spectra; this encompasses cool F- through early M-type stars. "Blue" stars have dominant Paschen series lines and virtually no Ca II triplet (i.e., O- through A-type stars).

Initially we anticipated using primarily late-type stars for our analysis, so that in the earlier runs (2002 March, 2003 March, and 2003 July observations; Table 1—Runs 1, 2, 3) we did not obtain "blue" standards. Later it became clear that good RVs for hotter stars could be derived and we began to collect blue standards. To cover the lack of blue standards in the earlier runs, the "blue" August 2003 standards were used to reduce all CTIO "blue" target stars. This approach was adopted and found to work moderately well because even across observing runs all spectra were taken with the same instrument setup, are dispersion corrected uniformly, and should experience no flexure problems because Hydra uses a bench-mounted spectrograph. In the end we did find some offsets in the RV zero-points for some of the runs—but, ironically these were for the runs where we actually did take blue standards (see Sections 3.6 and 3.7).

The standard star spectra (Table 2) provide a data set for calibration of the RV errors for each run according to Equations (1) and (2). Table 2 lists each observation of a standard star, the UT date of the observation (Column 2), its spectral type (Column 3), which observation frame and fiber were used (Columns 4 and 5), the TDR (Column 6), the mean derived radial velocity (V_r), and the measured standard deviation (Columns 7 and 8), followed by the average V_r and standard deviation for the cluster (Columns 9 and 10), also the IAU or Fekel (1999) RV is shown for comparison in Column 11. Using the Vogt et al. (1995) technique and measurements from Table 2, we find the parameters given in Table 3, which are used to determine errors

Table 4
Comparison of RV Standard Star Values

Star	Spectral type	UT date	V_r (km s^{-1})	$V_{r,\mathrm{IAU}}$ (km s^{-1})	Difference (km s^{-1})
HD 126053	G0V	2002 Mar 11	-20.8 ± 0.6	-18.5 ± 0.4	-2.3 ± 0.7
HD 150798	K2II-III	2002 Mar 11	-1.8 ± 0.8	-3.7 ± 0.2	$+1.9 \pm 0.8$
HD 157457	G8III	2002 Mar 12	$+17.7 \pm 0.6$	$+17.4 \pm 0.2$	$+0.3 \pm 0.7$
HD 136202	F8III-IV	2003 Mar 22	$+54.9 \pm 0.9$	$+53.5 \pm 0.2$	$+1.4 \pm 0.9$
HD 157457	G8III	2003 Mar 19	$+17.5 \pm 0.5$	$+17.4 \pm 0.2$	$+0.1 \pm 0.5$
HD 168454	K2.5IIIa	2003 Mar 19	-20.7 ± 0.4	-20.0 ± 0.0	-0.7 ± 0.4
HD 9138	K4III	2003 Jul 21	-34.2 ± 0.6	-35.4 ± 0.5	$+1.2 \pm 0.8$
HD 18884	M1.5IIIa	2003 Jul 21	-25.7 ± 1.5	-25.8 ± 0.1	$+0.1 \pm 1.5$
HD 9138	K4III	2003 Jul 22	-34.2 ± 0.3	-35.4 ± 0.5	$+1.2 \pm 0.6$
HD 18884	M1.5IIIa	2003 Jul 22	-25.8 ± 0.7	-25.8 ± 0.1	-0.0 ± 0.7
HD 107328	K0.5IIIb	2003 Jul 23	$+37.4 \pm 0.5$	$+35.7 \pm 0.3$	-1.7 ± 0.6
HD 146051	M0.5III	2003 Jul 23	-18.8 ± 0.8	-19.8 ± 0.0	$+1.0 \pm 0.8$
HD 693	F5V	2003 Aug 02	$+14.1 \pm 1.4$	$+14.7 \pm 0.2$	-0.6 ± 1.4
HD 9138	K4III	2003 Aug 02	-34.6 ± 0.6	-35.4 ± 0.5	$+0.8 \pm 0.8$
HD 18884	M1.5IIIa	2003 Aug 02	-25.7 ± 0.7	-25.8 ± 0.1	$+0.1 \pm 0.7$
HD 693	F5V	2003 Aug 03	$+14.8 \pm 1.6$	$+14.7 \pm 0.2$	$+0.1 \pm 1.6$
HD 18884	M1.5IIIa	2003 Aug 03	-25.5 ± 0.5	-25.8 ± 0.1	$+0.3 \pm 0.5$
HD 693	F5V	2003 Aug 05	$+14.4 \pm 1.0$	$+14.7 \pm 0.2$	-0.3 ± 1.0
HD 693	F5V	2003 Aug 06	$+14.8 \pm 2.1$	$+14.7 \pm 0.2$	$+0.1 \pm 2.1$
HR 7773	B9IV	2003 Aug 06	$+1.2 \pm 2.8$	-1.0 ± 0.2[a]	$+2.2 \pm 2.8$
HR 675	A2V	2003 Aug 07	-1.6 ± 4.5	$+0.4 \pm 0.2$[a]	-2.0 ± 4.5
HD 18884	M1.5IIIa	2003 Aug 07	-24.6 ± 1.4	-25.8 ± 0.1	$+1.2 \pm 1.4$
HD 693	F5V	2003 Aug 08	$+14.8 \pm 1.2$	$+14.7 \pm 0.2$	$+0.1 \pm 1.2$
HD 9138	K4III	2003 Aug 08	-34.7 ± 1.2	-35.4 ± 0.5	$+0.7 \pm 1.3$
HD 18884	M1.5IIIa	2003 Aug 08	-25.8 ± 1.2	-25.8 ± 0.1	$+0.0 \pm 1.2$

Note. [a] Stars HR 675 and HR 7773 are not IAU standards. Due to the lack of IAU standards hotter than F-type stars, we used stars from Fekel (1999).

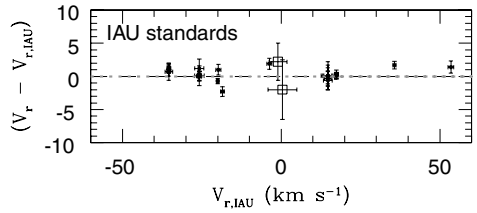

Figure 4. Comparison of the measured RVs for Fekel (1999, open boxes) and IAU radial velocity standard stars. The dashed line marks an ideal one-to-one correlation. The dotted line is a linear fit to the data.

for each of the runs. The variation in the α values can be due to the effects of focus and small spectrograph setup variations.

3.4. Radial Velocity Standard Verification

To check the reliability of our measurements of radial velocity standard stars, we compare the difference between our measurements (Table 4) and the IAU or Fekel (1999) values, as shown in Figure 4. As may be seen, the derived RVs for the standard stars are all within 2.3 km s^{-1} of the IAU values. We find that the differences between our measurement and the IAU values are no more than two times larger than the quadrature errors (as shown in Table 4); however, we find that the differences are randomly distributed and that the mean offset is less than 1 km s^{-1}. Therefore we find there are no systematic trends between our measured velocities and the cataloged values for the IAU standards, though we did find an offset for the "blue" Fekel (1999) stars, a situation that is analyzed in more depth below (Section 3.6).

3.5. Stellar Radial Velocities: Target Stars

Target stars were analyzed using the same reduction procedure as the standard stars, with the exception that stars that showed both the Paschen series lines and any hint of the Ca II triplet were considered "green" stars. As with the RV standards, the targets were sorted into "red," "blue," and "green" subsamples based on visual inspection of their spectral features in order to match them to the appropriate cross-correlation template. Figure 5(a) shows the 2MASS color distribution of the stars selected for each subsample. The "green" stars were tested against both templates to find the best match. Nearly all "green" stars became part of the "red" sample.

Each group of target stars was processed through IRAF's `fxcor` package to cross-correlate them against the standard of the corresponding color class for their respective observing run, as described in Section 3.3. "Green" stars were cross-correlated against both red and blue templates and the derived RV was taken from the template that provided the better result. The final 2MASS color distribution for stars fitted with the "red" and "blue" templates is shown in Figure 5(b). Uncertainties for the stars fitted to the "red" or "blue" templates were determined using the α values from Table 3 and Equation (1).

3.6. Internal Comparison (Red versus Blue)

As an additional check on the measured RVs, we tested the internal consistency delivered by the separate "red" and "blue" reductions for a given run. To do this, stars in our "green" sample were correlated with both the "red" and "blue" standards. For

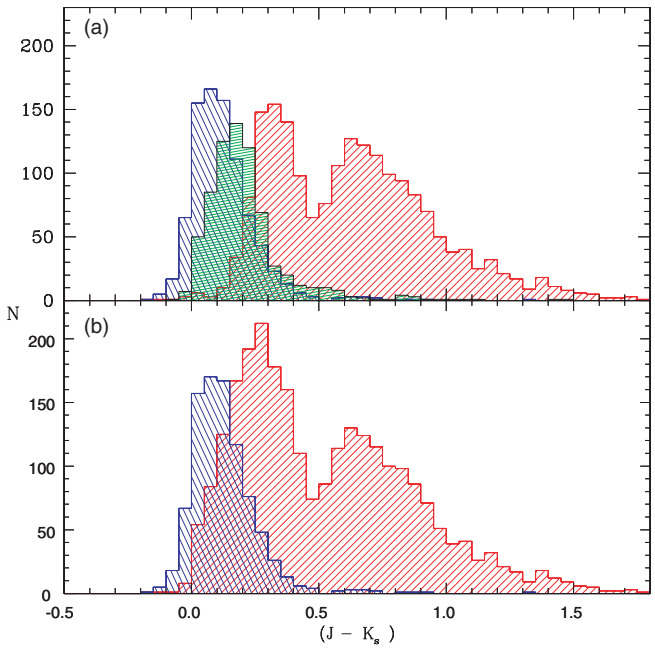

Figure 5. Comparison of the color/temperature of the cluster field stars to the selected RV template. (a) Raw selection of stars into "red," "green," and "blue" based on the appearance of the spectra. (b) The distribution of stars cross-correlated vs. IAU RV standards (red) and Fekel (1999) RV standards (blue).

Table 5
Comparison of Measured Red vs. Blue RVs

Run	a_0	a_1	RMS	Blue correction (km s^{-1})
2002 Mar	−0.47	0.97	3.06	0.0
2003 Mar	−1.26	0.99	3.74	−1.3
2003 Aug	−10.09	1.00	4.43	−10.0
2003 Sep	−6.05	0.98	4.63	−6.0

stars with measured uncertainties in their blue measurement of less than 10 km s^{-1}, Figure 6 shows ($V_{r,\mathrm{blue}} - V_{r,\mathrm{red}}$) versus $V_{r,\mathrm{red}}$, where stars with the best blue uncertainties ($\leqslant$6 km s^{-1}) are denoted with black squares. The subsample of stars with uncertainties of $\leqslant$6 km s^{-1} was then fitted with a line to determine if any zero point offset was needed between the red and blue samples. The fit to the data in the $V_{r,\mathrm{red}}$ versus $V_{r,\mathrm{blue}}$ plane is given by

$$V_{r,\mathrm{adopted}} = a_0 + a_1 * V_{r,\mathrm{blue}}. \quad (3)$$

The resulting fits for the 2002 March, 2003 March, 2003 August, and 2003 September runs are given in Table 5. We did not find a systematic difference between the $\leqslant$10 km s^{-1} and $\leqslant$6 km s^{-1} samples, just a larger scatter for the $\leqslant$10 km s^{-1} data.

We find that the blue data are offset from the red data by a significant amount for the August 2003 and September 2003 runs, and a small offset is found for the March 2003 run. To verify that it is the red values that are more reliable and to

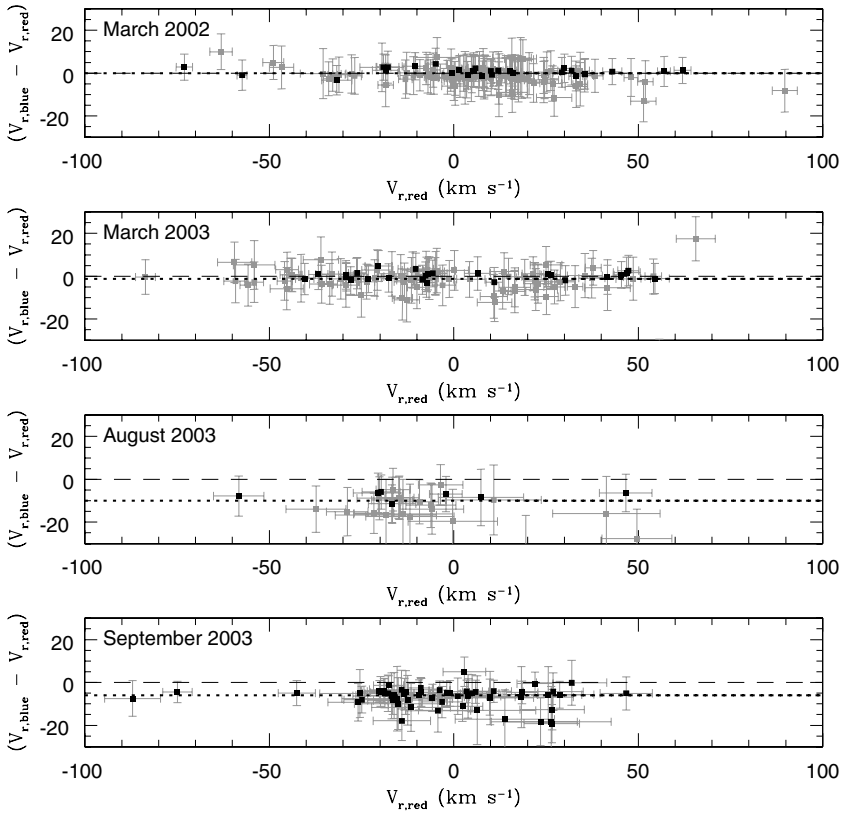

Figure 6. Comparison of RVs derived for the "green" spectra (which show both the Ca II triplet and the Paschen series features) using red vs. blue cross-correlation templates. All stars shown have RV measurement errors in the blue less than 10 km s^{-1}, the black squares have RV measurement errors in the blue less than 6 km s^{-1}. The black dashed line shows a perfect one-to-one correlation and the dotted line is a linear fit to the trends. (a) The 2002 March data show less than a 1 km s^{-1} shift, and therefore no offset was applied between the red and blue data. (b) 2003 March show a −1 km s^{-1} shift, which was applied to the "blue" RVs. (c) 2003 August show a −10 km s^{-1} shift, which was the correction applied to the "blue" RVs. (d) 2003 September show a −6 km s^{-1} shift, which was applied to the "blue" RVs. Note: the 2003 July run had no stars where the blue template error was less than 10 km s^{-1}.

Table 6
NGC 2682 Comparison to Previous RV Results

Star (*Tycho-2*)	SAND	FBC	MMJ	ES	α_{2000} (h)	δ_{2000} (°)	V_r (km s^{-1})	ϵ_{V_r} (km s^{-1})	$V_{r,\mathrm{Mathieu}}$ (km s^{-1})	ϵ_{V_r} (km s^{-1})	ΔV_r (km s^{-1})
0813-01125-1	0721	2554	6475	...	8:50:49.65	11:35:08.9	+33.01	0.79	+34.2	0.9	−1.2
0813-02302-1	0727	2425	5158	...	8:50:44.98	11:37:30.4	+21.44	1.82	+16.3	...	5.1
0814-02331-1	0978	3364	6482	...	8:51:17.48	11:45:22.7	+35.17	0.59	+34.7	0.6	0.5
0814-01531-1	1010	3536	6485	1008	8:51:22.81	11:48:01.8	+33.00	0.69	+33.6	0.4	−0.6
0814-01493-1	1016	3349	6484	...	8:51:17.10	11:48:16.2	+35.66	0.59	+34.3	0.7	1.4
0814-01631-1	1023	3668	6487	1001	8:51:26.84	11:48:40.5	+3.54	1.01	+3.6	1.0	−0.1
0814-01119-1	1040	3566	6488	...	8:51:23.78	11:49:49.4	+34.60	0.82	+32.0	6.3	2.6[a]
0814-01763-1	1054	3347	6489	4020	8:51:17.03	11:50:46.4	+32.63	0.72	+33.5	0.4	−0.9
0814-01099-1	1074	3204	6492	...	8:51:12.70	11:52:42.4	+34.50	0.68	+34.1	3.1	0.4
0814-01823-1	1221	4149	6497	...	8:51:43.56	11:44:26.4	+36.73	0.58	+34.1	3.1	2.6[a]
0814-01515-1	1250	3755	6499	...	8:51:29.91	11:47:16.8	+31.06	0.99	+34.3	1.4	−3.2
0814-01007-1	1277	4117	6502	3032	8:51:42.32	11:50:07.8	+33.18	0.78	+34.0	0.5	−0.8
0814-01147-1	1279	3726	6503	...	8:51:28.99	11:50:33.1	+33.93	0.66	+33.3	0.4	0.6
0814-01471-1	1288	4118	6505	3034	8:51:42.36	11:51:23.1	+32.25	0.67	+33.3	0.4	−1.0
0814-01225-1	1293	4039	6050	3035	8:51:39.38	11:51:45.4	+33.86	0.97	+34.1	0.5	−0.2
0814-00795-1	1306	...	...	3065	8:51:49.36	11:53:38.9	−2.44	0.63	−1.1	0.4	−1.3
0814-00134-1	1402	4878	6508	2152	8:52:10.97	11:31:49.2	+33.12	0.76	+33.6	0.4	−0.5
0814-00847-1	1327	3979	6507	3086	8:51:37.18	11:59:02.4	+11.62	0.87	+12.0	0.4	−0.4
0814-02313-1	1585	5191	...	...	8:52:26.33	11:41:27.7	+33.25	1.31	+34.1	0.1	−0.9

Notes.
References. SAND: Sanders (1977); FBC: Fan et al. (1996); MMJ: Montgomery et al. (1993); ES: Eggen & Sandage (1964); Mathieu: Mathieu et al. (1986).
[a] Star listed at spectroscopic binary in Mathieu et al. (1986).

support the rationale that we shift the blue system RVs to the red system, we next compare our RV measurements from the red sample with those of previously published, high RV resolution studies for a number of open clusters.

3.7. Systematic Effects and Comparison to Previous Results

As an additional test of the reliability of our RVs, we have found previously published values for stars in nine clusters that we have observed. We undertook a comparison of our velocity measures to those in the following studies: IC 4561 (Mermilliod et al. 1995; Meibom et al. 2002), IC 4756 (Mermilliod & Mayor 1990), NGC 2099 (Mermilliod et al. 1996), NGC 2423 (Mermilliod & Mayor 1990), NGC 2447 and NGC 2539 (Mermilliod & Mayor 1989), NGC 2682 (M67; Mathieu et al. 1986), NGC 5822 (Mermilliod & Mayor 1990), and NGC 6134 (Claria & Mermilliod 1992). In Table 6, we present a direct star-by-star comparison of RV results to the seminal work on M67 by Mathieu et al. (1986). Table 7 provides star-by-star comparison for the other clusters listed above, which include the *Tycho-2* star name, the star name from the corresponding photometry reference used for identification in the previous RV studies, the stellar coordinates, our RV (V_r) and its uncertainty, the reference RV and its uncertainty, and the per star difference in these measurements. For stars in common between the surveys, we find overall excellent agreement in the determined per star kinematics.

In Figure 7, we compare differences between our own red data and previously published RVs as a function of photometric parameters (e.g., magnitude and color) of the stars, where the data are color-coded by observing run (red = 2002 March, green = 2003 March, cyan = 2003 August, and blue = 2003 September). We find no systematic trend with magnitude or color, as shown in Figures 7(a)–(d). The bottom two plots in Figure 7 (panels e and f) show a comparison of ΔV_r versus V_r. While there may seem to be an odd trend at $-25 > V_r > -40$ km s^{-1} in panel (e), this is due mainly to one cluster—IC 4651—that has a peculiar offset. This is demonstrated by the "disappearance" of that odd trend when IC 4651 is removed from the distribution (Figure 7(f); see Section 6.2.2 for a detailed discussion of IC 4651).

Therefore, we find that our "red" sample, which we have made our standard reference, is consistent with previous work and this bears out our having corrected the blue sample RVs to the red RV system. The cause of this offset is probably due to a combination of using "blue" standards from different runs, as well as the fact that the two blue Fekel standard stars have only a few good lines for RV determination combined with large rotations with both Fekel stars having $V \sin i \sim 18$ km s^{-1}.

4. FINAL CLUSTER SAMPLE

Table 8 summarizes all clusters observed, including UT date of the observation and exposure times, the numbers of stars selected to be cluster members by Dias et al. (2001, 2002a) that were targeted with Hydra fibers (Column 4), the total number of stars and number of *Tycho-2* stars observed (Column 5), the number of total observed stars with reliable RVs (Column 6), and the *Tycho-2* stars with reliable RVs (Column 7). For the WIYN data, we were able to observe nearly 75–80% *Tycho-2* stars used in the corresponding Dias et al. (2001, 2002a) survey. For the CTIO runs, we found that we were generally able to observe 50–80% of the Dias et al. selected *Tycho-2* stars, and, in addition, sample an average of ∼50 more non-*Tycho-2* stars (since the latter were generally fainter by 1–3 magnitudes, a lower fraction of them delivered reliable velocities in the allotted observing time). Since we are obtaining data for most of the Dias et al. stars, we will be able to compare our new membership data directly against the membership analysis done by these authors (see Section 6.2.3).

Table 7
Star-by-Star Comparison to Previous Results

Star	α_{2000} (h)	δ_{2000} (°)	V_r (km s^{-1})	V_r (Other) (km s^{-1})	V_r (km s^{-1})	Other ID	Other references
			IC 4651				
8349-03672-1	17:24:06.77	−49:50:38.0	−55.31 ± 0.67	−52.9 ± 0.2	−2.4	2369	1
8349-03822-1	17:24:33.40	−49:54:56.0	−33.68 ± 0.61	−31.7 ± 0.5	−2.0	6333	1
8349-03822-1	17:24:33.40	−49:54:56.0	−33.68 ± 0.61	−30.9 ± 0.1	−2.8	6333	2
8349-03739-1	17:24:35.67	−49:56:27.0	−37.03 ± 0.67	−31.5 ± 0.0	−5.5[a]	6686	1
8349-03739-1	17:24:35.67	−49:56:27.0	−37.03 ± 0.67	−30.8 ± 0.1	−6.2[a]	6686	2
8349-03990-1	17:24:41.53	−49:59:06.3	−34.14 ± 0.66	−31.4 ± 0.1	−2.7	7646	1
8349-03990-1	17:24:41.53	−49:59:06.3	−34.14 ± 0.66	+31.2 ± 0.1	−2.9	7646	2
8349-03827-1	17:24:47.39	−49:50:19.1	−33.88 ± 0.70	−30.6 ± 0.2	−3.3[a]	8665	1
8349-03827-1	17:24:47.39	−49:50:19.1	−33.88 ± 0.70	+30.5 ± 0.2	−3.4	8665	2
8349-03909-1	17:24:50.08	−49:56:56.1	−33.62 ± 0.65	−30.9 ± 0.1	−2.7	9122	1
8349-03909-1	17:24:50.08	−49:56:56.1	−33.62 ± 0.65	−30.6 ± 0.1	−3.0	9122	2
8349-03395-1	17:24:51.50	−49:59:39.4	−37.31 ± 0.99	−31.5 ± 1.2	−5.8	9357	2
8349-03506-1	17:24:52.58	−49:56:31.4	−33.12 ± 1.39	−28.3 ± 0.7	−4.8	9536	2
8349-03284-1	17:24:54.14	−49:53:07.4	−33.79 ± 0.56	−31.6 ± 0.1	−2.2	9791	1
8349-03284-1	17:24:54.14	−49:53:07.4	−33.79 ± 0.56	−31.4 ± 0.1	−2.4	9791	2
8349-04025-1	17:24:57.75	−50:01:32.8	−34.71 ± 0.67	−31.9 ± 0.2	−2.8	10393	1
8349-04025-1	17:24:57.75	−50:01:32.8	−34.71 ± 0.67	−31.5 ± 0.1	−3.2	10393	2
8349-02900-1	17:25:04.49	−49:53:53.7	−35.38 ± 1.99	−28.0 ± 0.6	−7.4[a]	11504	2
8349-03017-1	17:25:08.94	−49:53:57.0	−31.37 ± 0.76	−30.1 ± 0.2	−1.3	12227	1
8349-03017-1	17:25:08.94	−49:53:57.0	−31.37 ± 0.76	−29.8 ± 0.1	−1.6	12227	2
8349-03472-1	17:25:13.21	−49:59:29.4	−33.09 ± 0.65	−30.1 ± 0.2	−3.0	12935	1
8349-03472-1	17:25:13.21	−49:59:29.4	−33.09 ± 0.65	−29.9 ± 0.1	−3.2	12935	2
8349-02891-1	17:25:21.78	−49:52:58.8	−22.51 ± 0.60	−31.6 ± 0.1	+9.1[a]	14290	1
8349-02891-1	17:25:21.78	−49:52:58.8	−22.51 ± 0.60	−31.4 ± 0.1	+8.9[a]	14290	2
8349-03516-1	17:25:23.53	−49:55:47.0	−30.44 ± 0.73	−32.5 ± 0.2	+2.1	14527	1
8349-03516-1	17:25:23.53	−49:55:47.0	−30.44 ± 0.73	−31.9 ± 0.3	+1.5	14527	2
8349-03480-1	17:25:24.38	−49:58:52.6	−35.07 ± 0.72	−31.5 ± 0.1	−3.6[a]	14641	1
8349-03480-1	17:25:24.38	−49:58:52.6	−35.07 ± 0.72	−31.2 ± 0.1	−3.9[a]	14641	2
			IC 4756				
0455-00950-1	18:37:30.30	5:12:15.7	−24.93 ± 1.27	−26.61 ± 0.17	+1.7	44	3
0455-00434-1	18:37:32.33	5:17:22.5	−27.33 ± 0.74	−22.53 ± 0.17	−4.8	48	3
0455-00376-1	18:37:34.22	5:28:33.5	−26.55 ± 1.14	−25.91 ± 0.19	−0.6	49	3
0455-00136-1	18:37:35.83	5:15:37.9	−26.80 ± 1.13	−25.87 ± 0.14	−0.9	52	3
0455-01014-1	18:38:05.16	5:24:33.8	−27.72 ± 1.40	−25.47 ± 0.08	−2.3[a]	69	3
0459-01415-1	18:38:17.58	5:38:17.1	−24.71 ± 1.27	−29.13 ± 0.66	+4.4[a]	80	3
0455-01297-1	18:38:20.76	5:26:02.3	−24.26 ± 1.29	−23.77 ± 0.13	−0.5	81	3
0455-00206-1	18:38:22.24	5:34:29.7	+33.15 ± 1.10	+32.29 ± 0.24	+0.9	82	3
0455-01170-1	18:38:43.79	5:14:20.0	−25.81 ± 1.21	−26.41 ± 0.19	+0.6	101	3
0455-00242-1	18:38:52.93	5:20:16.6	−23.35 ± 1.60	−25.92 ± 0.18	+2.6	109	3
			NGC 2099				
2410-01965-1	5:51:50.49	+32:31:53.9	+8.01 ± 0.60	+07.63 ± 0.10	+0.4[a]	412	4
2410-01612-1	5:51:55.15	+32:30:03.0	+9.80 ± 1.41	+08.61 ± 0.19	+1.2	401	4
2410-00460-1	5:52:02.27	+32:30:44.1	+7.87 ± 0.58	+09.66 ± 0.12	−1.8	277	4
2410-00950-1	5:52:08.07	+32:30:33.4	+8.49 ± 0.91	+08.21 ± 0.19	+0.3	148	4
2410-01091-1	5:52:24.15	+32:28:44.0	+35.51 ± 6.54	+06.65 ± 0.65	+28.9	255	4
2410-01397-1	5:52:40.62	+32:32:15.3	+11.93 ± 2.27	+08.07 ± 0.21	+3.9	350	4
2410-00572-1	5:52:46.55	+32:34:07.3	+15.31 ± 0.60	+08.64 ± 0.10	+6.7[a]	485	4
2410-00819-1	5:53:02.07	+32:24:37.0	+20.16 ± 0.70	+21.05 ± 0.38	−0.9	1006	4
			NGC 2423				
5409-02490-1	7:36:58.99	−13:54:55.9	+17.98 ± 0.57	+17.74 ± 0.16	+0.2	15	3
5409-02965-1	7:37:00.26	−13:45:37.9	+18.05 ± 0.66	+18.09 ± 0.23	+0.0	73	3
5409-03295-1	7:37:12.59	−13:44:55.2	+18.33 ± 0.63	+18.41 ± 0.35	−0.1[a]	70	3
5409-03708-1	7:37:28.58	−13:55:58.4	+19.13 ± 0.57	+18.81 ± 0.20	+0.3	56	3
5409-02736-1	7:37:55.50	−13:48:57.7	+28.81 ± 0.61	+29.60 ± 0.19	−0.8	60	3
			NGC 2447				
6540-03570-1	7:44:18.46	−23:53:23.7	+22.41 ± 0.40	+20.81 ± 0.13	+1.6	3	5
6540-03286-1	7:44:25.73	−23:49:53.0	+23.13 ± 0.50	+21.51 ± 0.21	+1.6	41	5
6540-04450-1	7:44:24.57	−23:50:44.0	+22.20 ± 0.67	+15.04 ± 1.21	+7.2[a]	42	5
6540-02684-1	7:44:44.18	−23:47:22.2	+22.80 ± 0.62	+22.65 ± 0.25	+0.2	93	5
6540-03594-1	7:44:53.81	−23:53:15.1	+27.71 ± 0.66	+20.90 ± 0.36	+6.8[a]	26	5
			NGC 2539				
5434-01183-1	8:10:15.18	−12:50:41.1	+27.42 ± 0.51	+29.18 ± 0.25	−1.8	(65)	5
5434-02548-1	8:10:23.02	−12:50:43.2	+27.74 ± 0.76	+29.95 ± 0.23	−2.2	(69)	5
5434-01219-1	8:10:42.86	−12:40:11.6	+28.67 ± 0.52	+29.08 ± 0.23	−0.4	26	5

Table 7
(Continued)

Star	α_{2000} (h)	δ_{2000} (°)	V_r (km s^{-1})	V_r (Other) (km s^{-1})	V_r (km s^{-1})	Other ID	Other references
			NGC 5822				
8681-01917-1	15:03:15.84	−54:16:39.1	−30.01 ± 0.61	−29.82 ± 0.19	−0.2	375	3
8685-00414-1	15:03:41.34	−54:22:32.8	−24.69 ± 0.52	−29.86 ± 1.03	+5.2[a]	2	3
8681-01417-1	15:04:02.26	−54:20:21.0	−30.98 ± 0.59	−31.48 ± 0.16	+0.5	1	3
8685-01594-1	15:04:12.73	−54:25:00.7	−27.11 ± 0.54	−32.22 ± 0.41	+5.1[a]	4	3
8685-01782-1	15:04:14.19	−54:25:47.3	−29.35 ± 0.64	−31.81 ± 0.60	+2.5[a]	3	3
8685-00456-1	15:04:21.25	−54:23:05.6	−30.26 ± 0.70	−29.68 ± 0.25	−0.6	6	3
8685-00712-1	15:04:30.39	−54:31:44.8	−30.57 ± 0.56	−29.95 ± 0.17	−0.6	240	3
8685-00872-1	15:04:35.95	−54:33:23.8	−40.49 ± 0.66	−31.03 ± 1.72	−9.5[a]	312	3
8681-00611-1	15:04:39.43	−54:21:04.0	−31.55 ± 0.67	−30.92 ± 0.22	−0.6	8	3
8681-01249-1	15:04:59.87	−54:17:55.1	+16.54 ± 0.57	+16.60 ± 0.17	−0.1	10	3
8685-00402-1	15:05:24.59	−54:22:59.3	−49.10 ± 0.52	−50.88 ± 0.20	+1.8	148	3
			NGC 6134				
8320-01143-1	16:27:32.21	−49:06:46.0	−24.88 ± 0.61	−25.76 ± 0.66	+0.8[a]	176	6
8320-01879-1	16:27:40.42	−49:11:39.0	−29.34 ± 3.38	−26.76 ± 0.49	−2.6	107	6
8320-01928-1	16:27:45.71	−49:07:33.5	−28.61 ± 0.62	−24.12 ± 0.54	−4.5[a]	30	6
8320-01904-1	16:27:46.11	−49:05:29.4	−25.89 ± 0.62	−26.08 ± 0.28	+0.2	129	6
8320-01799-1	16:27:51.01	−49:06:55.9	−28.72 ± 1.08	−26.17 ± 0.21	−2.6	79	6
8320-00960-1	16:27:56.29	−49:10:29.9	−24.82 ± 0.49	−24.92 ± 0.21	+0.1	99	6
8320-01695-1	16:28:00.18	−49:09:06.4	−29.19 ± 0.61	−29.29 ± 0.28	+0.1	91	6

References. (1) Mermilliod et al. (1995); (2) Meibom et al. (2002); (3) Mermilliod & Mayor (1990); (4) Mermilliod et al. (1996); (5) Mermilliod & Mayor (1989); (6) Claria & Mermilliod (1992). Other IDs are from the following references: IC 4651: Meibom et al. (2002); IC 4756: Kopff (1943); NGC 2099: van Zeipel & Lindgren (1921); NGC 2423: Hassan (1976); NGC 2447: Becker et al. (1976); NGC 2539: Pesch (1961); NGC 5822: Bozkert (1974); NGC 6134: Lindoff (1972).
[a] Star listed at spectroscopic binary.

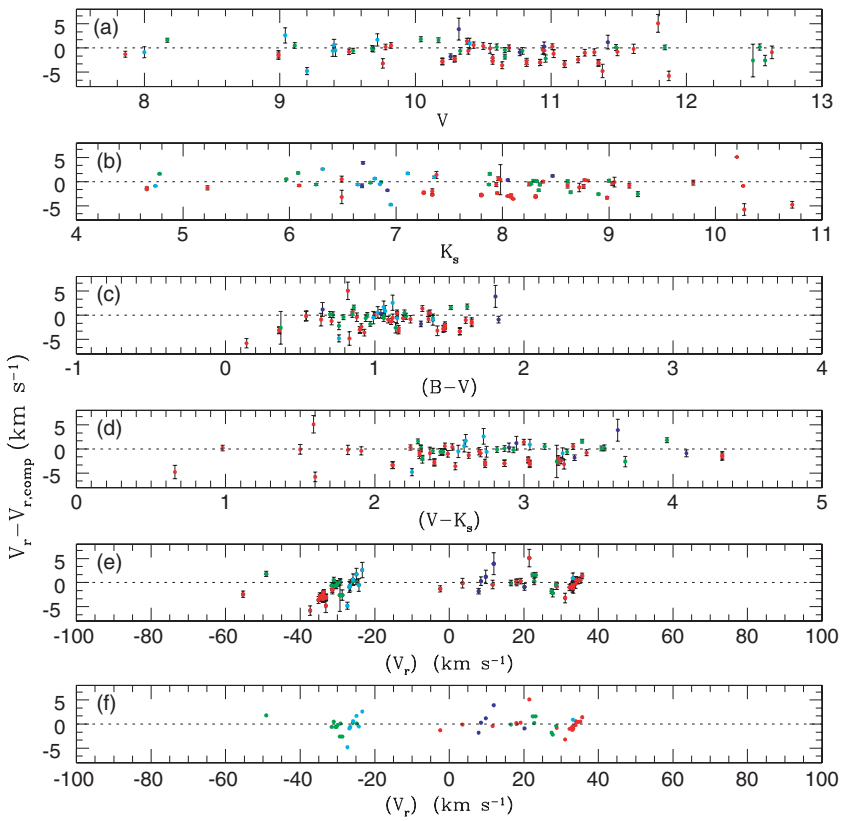

Figure 7. Comparison of our measured RVs vs. previously published star-by-star high-precision velocity results. All stars are color-coded by the observing run on which they were observed as follows: red = 2002 March; green = 2003 March; cyan = 2003 August; blue = 2003 September. (a) ΔV_r vs. the V magnitude converted from the Tycho (V_T) magnitude. (b) ΔV_r vs. the 2MASS K_s magnitude. (c) ΔV_r vs. the $(B - V)$ color converted from the Tycho (V_T, B_T) magnitudes. (d) ΔV_r vs. the $(V - K_s)$ color, where V is converted from the Tycho (V_T) and (K_s) is the 2MASS magnitude. (e) ΔV_r vs. our measured V_r. (f) The same as (e) except with cluster IC 4651 removed.

Table 8
Statistics of Observed Cluster Stars

Cluster	UT date	Exposures	$N_{\rm Dias}$	# Observed[a] (total/TYC)	# V_r Stars (total/TYC)
NGC 129	2003 Sep 15	3 × 600 s	29	67/29	29/29
NGC 381	2003 Sep 15	3 × 600 s	20	65/20	20/20
NGC 457	2003 Sep 17	3 × 600 s	17	61/17	17/17
NGC 884	2003 Sep 18	3 × 600 s	23	45/23	23/23
NGC 957	2003 Sep 16	3 × 600 s	19	63/19	19/19
NGC 1513	2003 Sep 15	3 × 600 s	19	48/19	19/19
NGC 1528	2003 Sep 17	3 × 600 s	43	43/43	43/43
NGC 1662	2003 Aug 07	3 × 600 s	13	108/13	70/13
Stock 8	2003 Sep 16	3 × 600 s	14	64/14	14/14
NGC 1960	2003 Sep 17	3 × 600 s	35	37/35	35/35
NGC 2099	2003 Sep 15	3 × 600 s	37	51/37	37/37
Kharchenko 1	2003 Sep 18	3 × 600 s	37	49/37	37/37
NGC 2215	2003 Mar 18	3 × 600 s	12	55/17	22/13
NGC 2264	2002 Mar 12	3 × 600 s	18	38/34	32/21
	2003 Mar 18	3 × 600 s		78/00	25/ 0
NGC 2301	2002 Mar 12	3 × 600 s	38	95/38	57/38
NGC 2323	2002 Mar 11	3 × 600 s	55	96/94	63/40
NGC 2354	2003 Mar 20	3 × 600 s	20	107/57	78/52
NGC 2353	2003 Mar 20	3 × 600 s	25	100/33	58/20
NGC 2423	2002 Mar 12	3 × 900 s	50	107/103	96/63
NGC 2437	2003 Mar 19	3 × 600 s	75	107/90	57/50
NGC 2447	2003 Mar 17	3 × 600 s	34	81/50	49/36
NGC 2482	2002 Mar 13	3 × 600 s	32	103/101	67/29
NGC 2516	2003 Mar 18	3 × 600 s	45	102/37	29/21
	2003 Mar 20	3 × 600 s		117/0	109/0
NGC 2527	2003 Mar 19	3 × 600 s	30	92/48	63/36
NGC 2546	2002 Mar 11	3 × 600 s	80	102/96	54/49
NGC 2547	2003 Mar 19	3 × 600 s	19	115/30	44/19
NGC 2539	2003 Mar 18	3 × 600 s	30	77/40	41/26
NGC 2548	2002 Mar 11	3 × 900 s	70	82/81	59/54
NGC 2567	2003 Mar 19	3 × 600 s	17	81/24	55/16
NGC 2579	2003 Mar 21	3 × 600 s	10	74/13	36/10
NGC 2670	2003 Mar 20	3 × 600 s	9	56/16	26/7
NGC 2669	2003 Mar 18	3 × 600 s	16	100/30	64/21
Trumpler 10	2002 Mar 14	3 × 900 s	22	87/32	49/20
NGC 2682	2002 Mar 14	3 × 600 s	28	109/28	65/28
Collinder 205	2003 Mar 19	3 × 600 s	12	67/14	32/9
IC 2488	2002 Mar 11	3 × 600 s	40	94/93	68/33
NGC 2925	2002 Mar 12	3 × 900 s	32	98/95	71/44
NGC 3680	2003 Mar 17	3 × 600 s	14	63/23	47/23
Collinder 258	2002 Mar 11	3 × 600 s	13	92/89	77/74
	2003 Mar 21	3 × 600 s		89/20	51/11
NGC 5281	2003 Mar 19	3 × 600 s	12	81/27	32/10
NGC 5316	2003 Mar 17	3 × 600 s	25	103/77	52/46
Lynga 1	2003 Mar 19	3 × 900 s	9	79/22	42/17
NGC 5460	2003 Mar 18	3 × 600 s	40	105/63	50/43
Lynga 2	2002 Mar 13	3 × 900 s	13	87/79	62/15
NGC 5617	2003 Mar 19	3 × 600 s	35	88/41	42/23
NGC 5662	2002 Mar 14	3 × 900 s	60	93/84	52/46
NGC 5822	2003 Mar 17	3 × 600 s	140	119/111	70/68
NGC 5823	2003 Mar 18	3 × 600 s	10	100/29	57/23
NGC 6025	2002 Mar 11	3 × 600 s	66	103/92	77/37
NGC 6031	2003 Mar 21	3 × 600 s	11	90/21	49/17
NGC 6067	2003 Mar 17	3 × 600 s	24	107/77	36/30
Harvard 10	2003 Mar 20	3 × 600 s	34	118/71	49/40
NGC 6124	2002 Mar 14	3 × 900 s	30	91/80	59/53
NGC 6134	2003 Mar 18	3 × 600 s	60	71/23	41/21
NGC 6167	2002 Mar 14	3 × 900 s	10	86/67	48/8
Ruprecht 119	2002 Mar 13	3 × 900 s	15	96/89	77/22
NGC 6250	2003 Aug 05	3 × 900 s	14	74/21	33/11
NGC 6281	2003 Mar 21	3 × 600 s	21	81/31	47/22
IC 4651	2002 Mar 13	3 × 900 s	19	96/77	78/30
NGC 6405	2003 Mar 21	3 × 600 s	30	110/51	70/50
NGC 6416	2003 Mar 21	3 × 600 s	32	100/63	52/34
NGC 6603	2003 Jul 21	3 × 600 s	22	110/39	55/23
IC 4756	2003 Aug 05	3 × 600 s	56	94/74	74/56
NGC 6705	2003 Aug 02	3 × 600 s	32	80/46	47/34
NGC 6811	2003 Sep 16	3 × 600 s	64	77/77	64/64
NGC 6866	2003 Sep 17	3 × 600 s	52	62/62	52/52
NGC 6885	2003 Aug 04	3 × 600 s	29	110/36	57/29
Berkeley 86	2003 Sep 16	3 × 600 s	46	67/67	46/46
Platais 1	2003 Sep 18	3 × 600 s	48	50/00	48/48
NGC 7209	2003 Sep 16	3 × 600 s	42	49/49	42/42
NGC 7654	2003 Sep 17	3 × 600 s	14	62/19	14/14

Note. [a] $N_{\rm Dias}$ is the number of *Tycho-2* stars observed, which are taken from the study of Dias et al. (2001, 2002a).

5. CLUSTER MEMBERSHIP ANALYSIS

One of the most complicated problems affecting studies of open clusters is membership contamination associated with their location within the densely populated Galactic plane. Large numbers of disk stars unrelated to the cluster lie along the CMD sequences of the typical open cluster and, given the typical motions of many objects within the Galactic plane, usually with rather similar velocities. To determine the bulk motion of clusters one must first isolate true cluster members from the dominant field star population in the fore/background. To accomplish this discrimination we have modified a previously implemented method designed to do just that. The star's proper motion, RV, and spatial distribution are all used as inputs for a kernel-based, probability distribution function technique, described below, that eventually allows the cluster bulk motion to be determined from stars with high membership probabilities.

5.1. Non-Parametric Frequency Function

To determine cluster membership probabilities for stars based on RV and proper motion, we have chosen to use an empirical, non-parametric technique—modified from that described in Galadí-Enríquez et al. (1998)—that incorporates a kernel estimator (Hand 1982) to isolate the phase space distribution of cluster stars in a field.

While we adopt the basic technique used by Galadí-Enríquez et al. (1998) for proper motions alone, we have generalized it also to operate on a spatially-constrained, 1D RV distribution as well as an RV-constrained, 2D proper motion distribution. In principle, one could use either distribution separately for culling cluster members, but for the most secure assessment of membership we depend on the joint probability distributions. This means, therefore, that we can only use stars having both RV and proper motion data. To improve our results further, we remove stars with large measurement errors in either proper motion or RV, or those stars that clearly have halo-like RVs, using the following constraints applied to the data:

$$\mu \text{ error limit: } \sqrt{\sigma^2_{\mu^*_\alpha} + \sigma^2_{\mu_\delta}} \leqslant 10 \text{ mas yr}^{-1}$$

$$\text{RV limit: } -200 < V_r < 200 \text{ km s}^{-1}$$

$$\text{RV error limit: } \sigma_{V_r} \leqslant 10 \text{ km s}^{-1}.$$

The modified version of the Galadí-Enríquez et al. (1998) formulation is intended to perform better for our particular survey circumstances—i.e., fewer numbers of stars per cluster, but high-quality RV data for these stars. Throughout the following

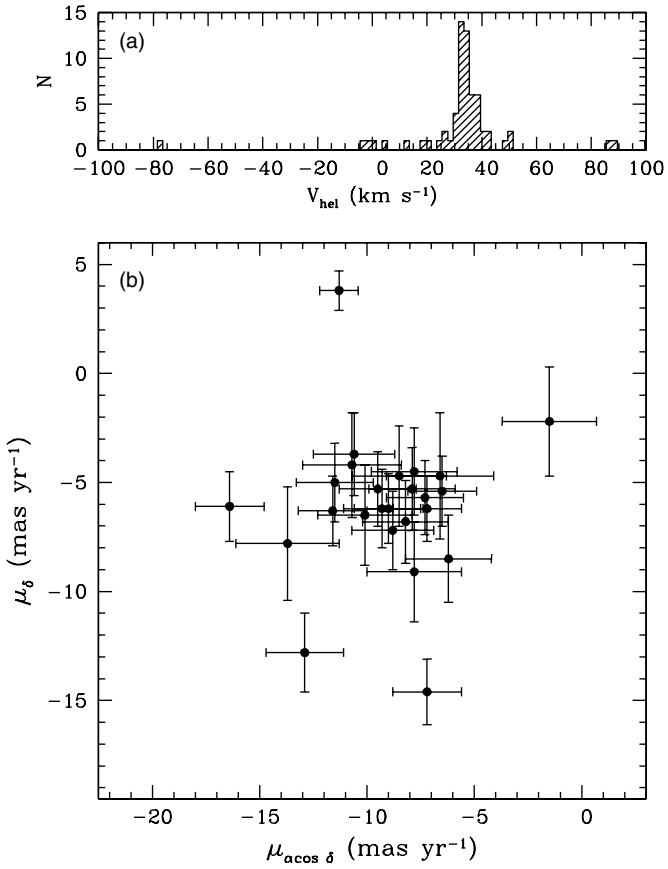

Figure 8. Our measured kinematical data for NGC 2682 (M67). (a) RV distribution, shown with 2 km s^{-1} binning, of all stars with RVs between −100 and +100 km s^{-1} measured for NGC 2682. (b) Proper motion distribution of all observed stars with proper motion data in the NGC 2682 field having *Tycho-2* data with error bars shown.

description we will demonstrate the basic features of our analysis via the example processing of the cluster NGC 2682 (M67), for which the raw data are shown in Figure 8.

5.2. 1D Kinematical Distribution: Radial Velocities

For our data, the RV distribution is found to be the most sensitive discriminator of cluster membership because of the small measured relative RV errors. When applying a kernel density estimator the empirical density function $\left(\psi^V_{c+f}\right)$ is comprised of both the cluster (c) and the field (f), where here V stands for the RV distribution. Since the observed empirical density function is the sum of two underlying distributions (e.g., $\psi^V_{c+f} = \psi^V_f + \psi^V_c$), one must decompose the distributions to isolate the cluster function. Because of the accuracy of the RV data and the small intrinsic velocity dispersions of open clusters (0.5–3 km s^{-1}), we expect to be able to discriminate the cluster and field fairly readily. To do so, however, we must first isolate the field population to verify which peak in the ψ^V_{c+f} distribution is due to the cluster. Differences in the cluster versus field distribution should be evident by looking at samples of stars drawn from different radii from the cluster center. A useful initial assumption is that stars outside of the cluster radius are "non-members," and these can provide a reasonable estimate of ψ^V_f.

The RV data kernel analysis is comprised of four steps: (1) all RV data are convolved with a Gaussian kernel to homogenize our errors for a given cluster. This kernel has a width determined by the mean RV errors from all of the observed stars in a given cluster field. Because open clusters have intrinsic velocity dispersions of 1–3 km s^{-1} in addition to our measurement errors, we limit the Gaussian width to be *at least* 3 km s^{-1} and at most 10 km s^{-1}. Applying the Gaussian kernel to smooth our RV data $\left(\psi^V_{c+f}\right)$ produces the smoothed field plus cluster distribution Ψ^V_{c+f}; an example for NGC 2682 (M67) is shown in Figure 9(a). (2) We apply the same Gaussian kernel to smooth the RV data of stars that are outside the cluster radius (utilizing the cluster diameters from Dias et al. 2002b). This smoothed RV distribution is used as the field distribution Ψ^V_f (Figure 9(b)). (3) We wish to determine the probability of any particular star with a given RV being a member of the cluster, so we need to determine the normalized probability distribution:

$$P^V_c(V_{r,i}) = \frac{\Psi^V_{c+f}(V_{r,i}) - \Psi^V_f(V_{r,i})}{\Psi^V_{c+f}(V_{r,i})}. \quad (4)$$

The cluster probability distribution P^V_c is shown Figure 9(c); however, we see that a few outliers, which are non-member stars within the cluster radius, are still visible in the distribution. (4) We assume that the strongest peak in the "cluster" probability distribution, P^V_c, belongs to the cluster, and perform a 1D Gaussian fit to this peak (Figure 9(d); dotted line). This Gaussian fit is used to determine RV membership probabilities, P^V_c, for all stars in the field and to exclude non-member RVs that still may appear in Ψ^V_c.

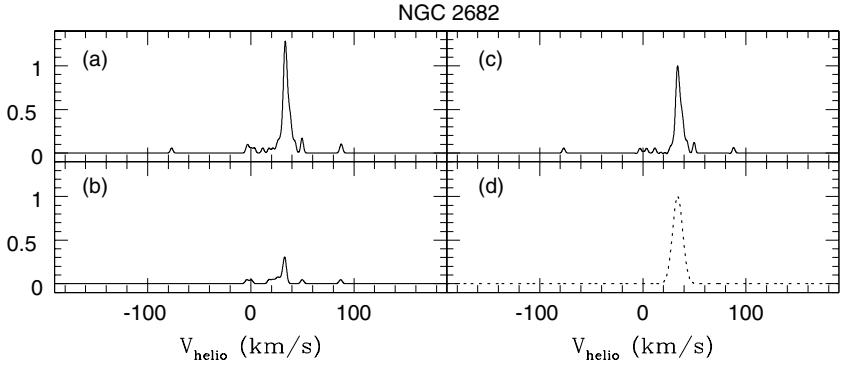

Figure 9. Steps in the membership analysis for NGC 2682 (M67) for the 1D RV distribution (V_r). (a) Kernel-smoothed RV distribution for all stars used in the analysis of the data for the cluster NGC 2682. (b) Kernel-smoothed distribution for stars not within the cluster radius (Dias et al. 2002b). (c) Probability distribution estimated by [(a)−(b)]/(a). (d) 1D Gaussian fit to (c). The fit to the "cluster" distribution used to determine the membership probability (P^V_c) based on the spatially-constrained RV data.

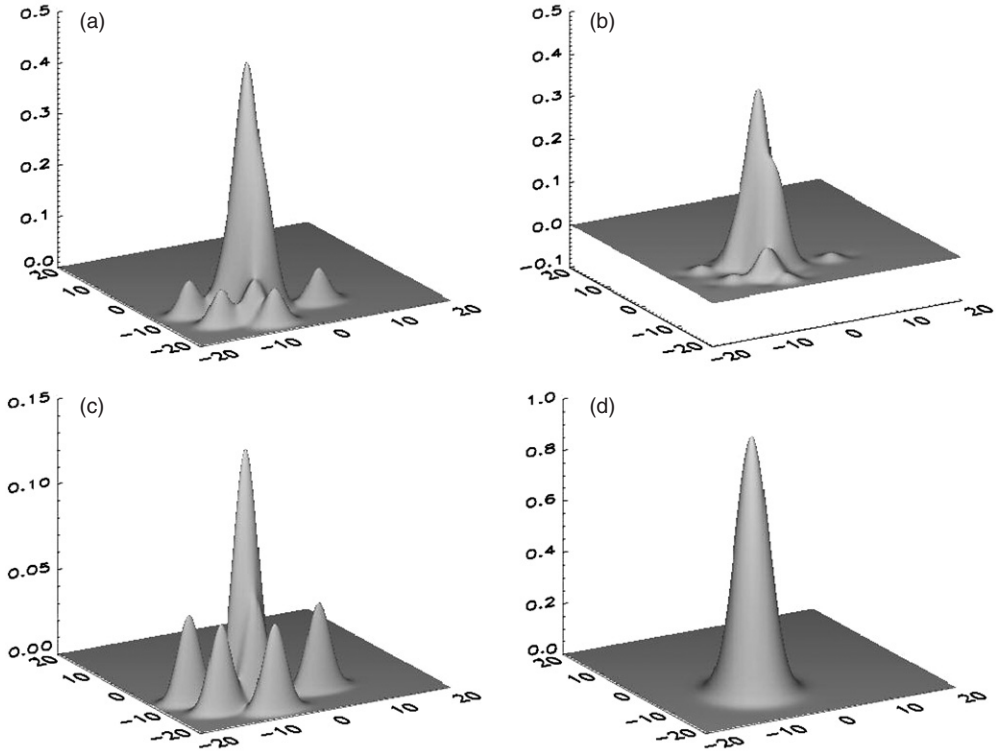

Figure 10. Steps in the analysis of the 2D proper motion distribution ($\mu_{\alpha\cos(\delta)}$, μ_δ) for NGC 2682 (M67). (a) Kernel-smoothed distribution of all stars used in the analysis. (b) Kernel-smoothed distribution for stars not selected to be RV members (see Figure 9; $P_c^V < 0.8$). (c) The probability distribution given by [(a)−(b)]/(a). (d) The normalized 2D Gaussian fit to the distribution in panel (c). The resulting fitted "cluster" distribution used to determine P_c^K.

5.3. 2D Kinematical Plane: Proper Motions

The proper motion kernel analysis is similarly comprised of four steps, but now applied in 2D. This technique for proper motions is identical to that used in Galadí-Enríquez et al. (1998) with the exception that instead of using a spatial membership separation (which we used for the RV distribution described above) to establish Ψ_f^K, we have chosen to use the RV separation described above (i.e., those stars outside the Gaussian fit to the RV distribution, $P_c^V = 0$, are considered the "field" population). The proper motion kernel uses the following equation analogous to that used in the RV analysis above:

$$P_c^K(\mu_{\alpha',i}, \mu_{\delta,j}) = \frac{\Psi_{c+f}^K(\mu_{\alpha',i}, \mu_{\delta,j}) - \Psi_f^K(\mu_{\alpha',i}, \mu_{\delta,j})}{\Psi_{c+f}^K(\mu_{\alpha',i}, \mu_{\delta,j})}, \quad (5)$$

where α' is $\alpha\cos(\delta)$. Continuing our example of NGC 2682, we apply the 2D kernel smoothing to the proper motion distribution as shown in Figures 10(a)–(d). The Gaussian fit to the field-subtracted distribution is used to determine proper motion membership probabilities P_c^K (Figure 10(d)) for stars in each cluster. Both the RV and proper motion kernel analysis was performed on all clusters in Table 6.

5.4. Calibration of the Membership Criteria

To determine the RV membership "cutoff" criteria, we have chosen to analyze in detail one of our best-sampled clusters, our example NGC 2682. Using techniques standard dynamical techniques from Pryor & Meylan (1993), we performed an iterative 3σ rejection using the full sample of NGC 2682 RV data. We find an intrinsic velocity dispersion of $\sigma_{\rm int} = 0.96 \pm 0.29$ km s^{-1}. As a comparison, using proper motions, Girard et al. (1989) found that NGC 2682 (M67) has $\sigma_{\rm int} = 0.81 \pm 0.10$ km s^{-1}. Comparing the RV member stars left after applying the iterative 3σ rejection, we find that all of the remaining stars have $P_c^V \geqslant 70\%$. More leniency is given to the proper motions

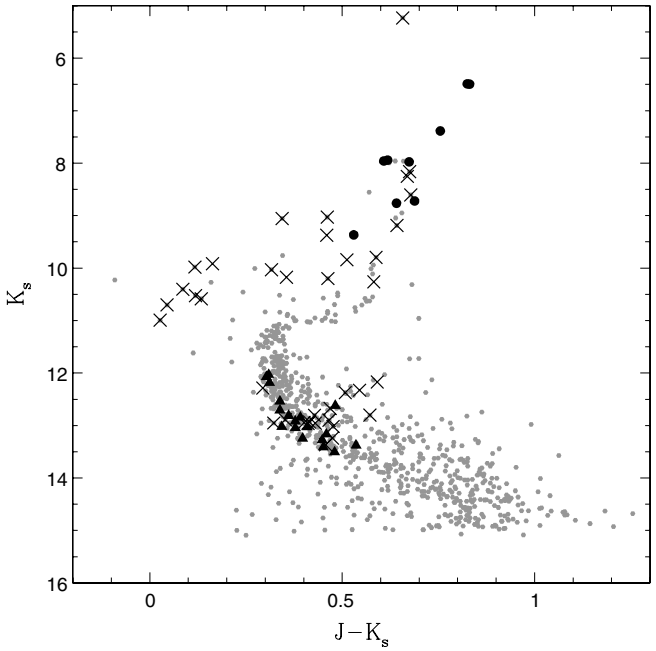

Figure 11. 2MASS CMD for NGC 2682 (M67) for stars inside the cluster radius (Dias et al. 2002b). Crosses (×) denote stars that we determined to be non-members. Large circles denote stars selected to be members based on *both* RV and proper motion criteria. Triangles denote stars that have $P_c^V > 70\%$ but which do not have *Tycho-2* proper motion data available.

Table 9
Cluster Analysis—NGC 2682 Example[a]

Star	α_{2000}	δ_{2000}	$\mu_\alpha \cos\delta$	μ_δ	V_r	Type[b]	Probabilities			
	(h)	(°)	(mas yr^{-1})	(mas yr^{-1})	(km s^{-1})		Dias	P_c^K	P_c^V	$P_c^{\rm tot}$
f9754-MMJ5132	8:50:42.52	11:39:49.7	...	...	33.53 ± 3.24	Red	c	0.0	100.0	0.0
0813-01521-1	8:50:43.57	11:35:48.8	25.9 ± 1.7	−32.7 ± 1.9	−3.84 ± 1.07	Red	0	0.0	0.0	0.0
0813-02302-1	8:50:44.98	11:37:30.4	−1.5 ± 2.2	−2.2 ± 2.5	21.44 ± 1.82	Red	0	1.3	4.5	0.0
H800-FBC2476	8:50:46.82	11:52:57.4	...	...	−76.71 ± 5.47	Red	c	0.0	0.0	0.0
0813-01125-1	**8:50:49.65**	**11:35:08.9**	**−6.5 ± 1.6**	**−5.4 ± 1.6**	**33.01 ± 0.79**	**Red**	**98**	**87.9**	**99.3**	**87.3**
H822-FBC2800	8:50:58.41	11:58:14.4	...	...	31.22 ± 4.30	Red	c	0.0	88.7	0.0
0813-02294-1	8:51:03.51	11:45:02.7	−8.8 ± 1.9	−7.2 ± 1.8	38.36 ± 2.04	Red	99	72.1	63.1	45.5
H801-FBC3002	8:51:05.82	11:53:10.7	...	...	39.19 ± 4.44	Red	c	0.0	53.3	0.0
H724-FBC3017	8:51:06.50	11:35:59.0	...	...	37.66 ± 2.94	Red	c	0.0	71.7	0.0
H942-FBC3059	8:51:07.99	11:38:26.5	...	...	201.79 ± 2.65	Red	c	0.0	0.0	0.0
H1095-FBC3099	8:51:09.20	11:57:01.0	...	...	37.16 ± 1.77	Red	c	0.0	77.5	0.0
H1002-ES1013	8:51:12.23	11:47:15.0	...	...	35.91 ± 4.55	Red	c	0.0	89.6	0.0
0814-01099-1	**8:51:12.70**	**11:52:42.4**	**−7.8 ± 2.0**	**−4.5 ± 2.0**	**34.50 ± 0.68**	**Red**	**98**	**90.0**	**98.7**	**88.8**
H1096-FBC3210	8:51:13.10	11:57:01.0	...	...	33.92 ± 2.25	Red	c	0.0	99.8	0.0
0814-01931-1	8:51:14.35	11:45:00.5	−12.9 ± 1.8	−12.8 ± 1.8	39.64 ± 1.38	Red	0	0.0	47.3	0.0
0814-01448-1	8:51:14.74	11:30:09.9	36.5 ± 2.4	−164.5 ± 2.5	49.87 ± 0.76	Red	c	0.0	0.0	0.0
0814-01763-1	8:51:17.03	11:50:46.4	−10.1 ± 2.2	−6.5 ± 2.3	32.63 ± 0.72	Red	99	56.5	97.9	55.4
0814-01493-1	**8:51:17.10**	**11:48:16.2**	**−8.2 ± 2.0**	**−6.8 ± 1.9**	**35.66 ± 0.59**	**Red**	**99**	**86.4**	**92.0**	**79.5**
0814-02331-1	**8:51:17.48**	**11:45:22.7**	**−7.3 ± 1.8**	**−5.7 ± 1.7**	**35.17 ± 0.59**	**Red**	**99**	**98.5**	**95.4**	**94.0**
H966-FBC3503	8:51:21.85	11:43:17.8	...	...	28.84 ± 3.98	Red	c	0.0	61.9	0.0
H1079-FBC3505	8:51:21.96	11:53:09.1	...	...	34.84 ± 4.40	Red	c	0.0	97.0	0.0
0814-01531-1	**8:51:22.81**	**11:48:01.8**	**−7.9 ± 2.0**	**−5.3 ± 1.9**	**33.00 ± 0.69**	**Red**	**99**	**98.9**	**99.0**	**97.9**
0814-01119-1	**8:51:23.78**	**11:49:49.4**	**−6.6 ± 2.5**	**−4.7 ± 2.9**	**34.60 ± 0.82**	**Red**	**97**	**83.9**	**98.3**	**82.5**
0814-01911-1	8:51:26.43	11:43:50.7	−9.3 ± 1.8	−6.2 ± 1.8	40.96 ± 2.17	Red	99	77.6	33.0	25.6
0814-01631-1	8:51:26.84	11:48:40.5	−16.4 ± 1.6	−6.1 ± 1.6	3.54 ± 1.01	Red	0	0.0	0.0	0.0
0814-01205-1	8:51:27.01	11:51:52.6	−9.0 ± 1.6	−6.2 ± 1.6	49.93 ± 2.94	Red	99	83.7	0.0	0.0
H943-FBC3716	8:51:28.61	11:38:32.0	...	...	26.67 ± 1.95	Red	c	0.0	36.0	0.0
H1215-FBC3720	8:51:28.92	11:43:08.9	...	...	32.13 ± 4.44	Red	c	0.0	95.4	0.0
0814-01147-1	**8:51:28.99**	**11:50:33.1**	**−9.5 ± 1.8**	**−5.3 ± 1.7**	**33.93 ± 0.66**	**Red**	**99**	**74.9**	**99.8**	**74.8**
0814-01515-1	**8:51:29.91**	**11:47:16.8**	**−7.2 ± 1.6**	**−6.2 ± 1.5**	**31.06 ± 0.99**	**Red**	**99**	**94.8**	**86.9**	**82.4**
H1341-FBC3789	8:51:30.80	12:04:16.0	...	...	32.23 ± 2.24	Red	c	0.0	96.0	0.0
H1229-GBDS101	8:51:31.77	11:45:09.0	...	...	32.88 ± 3.05	Red	c	0.0	98.7	0.0
H1246-ES2010	8:51:32.41	11:46:45.8	...	...	37.78 ± 2.09	Red	c	0.0	70.5	0.0
0814-02087-1	8:51:32.59	11:48:52.1	−11.5 ± 1.8	−5.0 ± 1.8	36.07 ± 1.74	Red	94	27.7	88.7	24.5
H1208-FBC3856	8:51:32.60	11:42:05.0	...	...	37.66 ± 5.97	Red	c	0.0	71.7	0.0
H1236-ES2019	8:51:33.38	11:45:59.9	...	...	33.96 ± 2.33	Red	c	0.0	99.8	0.0
H1184-FBC3937	8:51:35.53	11:34:32.1	...	...	33.87 ± 4.93	Red	c	0.0	99.9	0.0
0814-00847-1	8:51:37.18	11:59:02.4	−29.2 ± 2.0	−2.1 ± 2.0	11.62 ± 0.87	Red	0	0.0	0.0	0.0
f9756-FBC3985	8:51:37.37	12:03:19.8	...	...	24.96 ± 5.32	Red	c	0.0	20.7	0.0
0814-01225-1	8:51:39.38	11:51:45.4	−7.8 ± 2.2	−9.1 ± 2.3	33.86 ± 0.97	Red	92	34.5	99.9	34.5
0814-01007-1	8:51:42.32	11:50:07.8	−10.7 ± 2.3	−4.2 ± 2.4	33.18 ± 0.78	Red	96	38.6	99.5	38.4
0814-01471-1	**8:51:42.36**	**11:51:23.1**	**−8.5 ± 2.2**	**−4.7 ± 2.3**	**32.25 ± 0.67**	**Red**	**99**	**88.2**	**96.0**	**84.6**
0814-01823-1	8:51:43.56	11:44:26.4	−6.2 ± 2.0	−8.5 ± 2.0	36.73 ± 0.58	Red	89	39.6	81.9	32.4
f9750-FBC4138	8:51:44.96	11:38:59.3	...	...	32.63 ± 1.49	Red	c	0.0	97.9	0.0
0814-00264-1	8:51:46.09	11:36:18.8	−12.8 ± 1.6	−59.8 ± 1.6	87.07 ± 0.75	Red	0	0.0	0.0	0.0
H1249-ES2042	8:51:47.45	11:47:09.8	...	...	42.90 ± 2.00	Red	c	0.0	17.2	0.0
H1211-FBC4291	8:51:48.48	11:42:23.7	...	...	35.12 ± 2.47	Red	c	0.0	95.4	0.0
0814-02047-1	8:51:48.64	11:49:15.6	−11.6 ± 1.6	−6.3 ± 1.6	42.85 ± 2.10	Red	95	25.6	17.2	4.4
H1251-ES2041	8:51:48.70	11:47:35.8	...	...	88.25 ± 2.74	Red	c	0.0	0.0	0.0
0814-00795-1	8:51:49.36	11:53:38.9	−11.3 ± 0.9	3.8 ± 0.9	−2.44 ± 0.63	Red	0	0.0	0.0	0.0
f9773-SAND1507	8:51:51.78	12:04:47.1	...	...	32.99 ± 1.96	Red	c	0.0	99.0	0.0
H1484-FBC4433	8:51:53.30	11:56:17.0	...	...	31.98 ± 3.57	Red	c	0.0	94.2	0.0
0814-02253-1	8:51:54.91	11:40:26.8	−22.3 ± 1.6	−45.8 ± 1.6	49.30 ± 0.78	Red	0	0.0	0.0	0.0
0814-01011-1	8:51:56.01	11:51:26.6	−7.2 ± 1.6	−14.6 ± 1.5	29.79 ± 2.21	Red	0	0.0	72.9	0.0
H1422-FBC4502	8:51:56.10	11:39:14.0	...	...	27.05 ± 5.68	Red	c	0.0	40.4	0.0
H1473-FBC4508	8:51:56.24	11:53:35.9	...	...	35.59 ± 2.92	Red	c	0.0	92.8	0.0
H1449-FBC4515	8:51:56.61	11:47:25.0	...	...	33.59 ± 3.47	Red	c	0.0	100.0	0.0
H1468-FBC4578	8:51:58.65	11:52:15.0	...	...	38.84 ± 2.83	Red	c	0.0	56.9	0.0
H1492-FBC4654	8:52:01.59	12:01:03.2	...	...	17.73 ± 4.11	Red	c	0.0	0.0	0.0
H1452-FBC4706	8:52:03.51	11:47:48.0	...	...	34.78 ± 3.23	Red	c	0.0	97.5	0.0
H1414-FBC4777	8:52:06.37	11:37:30.7	...	...	0.42 ± 2.26	Red	c	0.0	0.0	0.0

Table 9
(Continued)

Star	α_{2000}	δ_{2000}	$\mu_\alpha \cos\delta$	μ_δ	V_r	Type[b]	Probabilities			
	(h)	(°)	(mas yr^{-1})	(mas yr^{-1})	(km s^{-1})		Dias	P_c^K	P_c^V	$P_c^{\rm tot}$
0814-00134-1	8:52:10.97	11:31:49.2	-10.6 ± 1.9	-3.7 ± 1.9	33.12 ± 0.76	Red	94	35.2	99.5	35.0
H1426-FBC4887	8:52:11.40	11:40:32.0	...	...	31.94 ± 3.44	Red	c	0.0	94.2	0.0
H1601-FBC5015	8:52:16.90	11:48:31.0	...	...	29.86 ± 6.40	Red	c	0.0	74.0	0.0
0814-02313-1	8:52:26.33	11:41:27.7	-13.7 ± 2.4	-7.8 ± 2.6	33.25 ± 1.31	Red	21	2.9	99.7	2.9

Notes.
[a] Boldface entries denote star selected as cluster members using the 3D criteria.
[b] Type of spectral template used in the cross-correlation for RV determination, as described in Section 3.3.
[c] Star not used in Dias et al. (2001) membership analysis.

Table 10
Cluster Analysis—All Data[a]

Star	α_{2000}	δ_{2000}	$\mu_\alpha \cos\delta$	μ_δ	V_r	Type[b]	Probabilities			
	(h)	(°)	(mas yr^{-1})	(mas yr^{-1})	(km s^{-1})		Dias	P_c^K	P_c^V	$P_c^{\rm tot}$
Berkeley 86										
3151-02453-1	20:17:17.981	38:30:15.903	-15.5 ± 2.9	-14.1 ± 2.8	6.57 ± 0.89	Red	0	0.0	0.0	0.0
3151-00710-1	20:17:20.618	38:47:21.298	-4.9 ± 1.9	-3.1 ± 1.8	-30.10 ± 0.77	Blue	95	77.3	63.1	48.8
3151-01565-1	20:17:20.783	38:37:20.099	-10.7 ± 1.7	-5.8 ± 1.7	29.95 ± 5.81	Red	32	1.6	0.0	0.0
3151-02271-1	20:17:32.071	38:22:30.206	0.6 ± 1.4	14.6 ± 1.4	-15.01 ± 1.29	Red	0	0.0	10.5	0.0
3151-01751-1	20:17:34.962	38:33:37.104	-4.5 ± 1.4	-5.2 ± 1.4	-70.35 ± 3.07	Blue	96	92.9	0.0	0.0
3151-02729-1	20:17:37.702	38:24:48.496	-2.9 ± 4.2	-5.5 ± 3.9	22.06 ± 0.55	Red	94	84.1	0.0	0.0
3151-00572-1	20:17:43.037	38:36:10.500	-2.5 ± 1.1	-7.5 ± 1.1	-33.90 ± 1.73	Blue	88	38.6	22.2	8.6
3151-02900-1	20:17:44.980	38:24:25.700	-5.8 ± 2.1	-4.0 ± 2.0	-37.57 ± 4.04	Blue	95	71.5	4.7	3.4
3151-03253-1	20:17:56.131	38:47:13.498	-0.4 ± 1.3	14.0 ± 1.3	-39.62 ± 0.50	Red	0	0.0	1.5	0.0
3151-03071-1	20:17:58.150	38:21:07.603	-5.4 ± 2.4	-1.8 ± 2.5	-411.00 ± 6.74	Blue	91	43.7	0.0	0.0

Notes.
[a] Boldface entries denote star selected as cluster members using the 3D criteria.
[b] Type of spectral template used in the cross-correlation for RV determination, as described in Section 3.3.
[c] Star not used in Dias et al. (2001) membership analysis.
[d] Star not analyzed due to large errors (see Section 5.1).
(This table is available in its entirety in machine-readable and Virtual Observatory (VO) forms in the online journal. A portion is shown here for guidance regarding its form and content.)

Table 11
2MASS and *Tycho-2* Photometry for Targeted Cluster Stars

Star	2MASS ID	α_{2000}	δ_{2000}	B_{Tycho}	V_{Tycho}	2MASS J	2MASS H	2MASS K_s	3D Memb?
Berkeley 86									
3151-02453-1	20171796+3830158	20:17:17.98	38:30:15.9	12.12	11.82	10.54	10.29	10.24	N
3151-00710-1	20172062+3847214	20:17:20.62	38:47:21.3	11.93	11.38	10.46	10.41	10.32	N
3151-01565-1	20172080+3837200	20:17:20.78	38:37:20.1	11.37	11.12	10.00	9.86	9.76	N
3151-02271-1	20173206+3822302	20:17:32.07	38:22:30.2	11.01	10.82	9.96	9.82	9.79	N
3151-01751-1	20173495+3833369	20:17:34.96	38:33:37.1	10.30	10.07	9.62	9.53	9.42	N
3151-02729-1	20173769+3824484	20:17:37.70	38:24:48.5	13.19	11.31	7.92	7.10	6.87	N
3151-00572-1	20174304+3836104	20:17:43.04	38:36:10.5	9.12	9.02	8.81	8.85	8.86	N
3151-02900-1	20174496+3824255	20:17:44.98	38:24:25.7	12.59	12.10	11.02	10.90	10.87	N
3151-03253-1	20175612+3847137	20:17:56.13	38:47:13.5	11.10	9.78	7.84	7.33	7.22	N
3151-03071-1	20175815+3821074	20:17:58.15	38:21:07.6	11.87	11.75	10.54	10.45	10.39	N

Note. [a] Star not matched to any 2MASS point source.
(This table is available in its entirety in machine-readable and Virtual Observatory (VO) forms in the online journal. A portion is shown here for guidance regarding its form and content.)

due to the larger average error, and in this regard we follow the criterion used by Dias et al. (2001, 2002a). As a result, we have chosen to define cluster membership as stars that have $P_c^V > 70\%$ and $P_c^K > 51\%$.

5.5. Results of the Membership Analysis

Cluster membership was determined by jointly assessing the probabilities from the 1D RV distribution $\left(P_c^V\right)$ and the 2D proper motion distribution $\left(P_c^K\right)$. The probabilities for each star analyzed in the cluster NGC 2682 are included along with the RV and proper motion data in Table 9. This table includes the star name from the *Tycho-2* survey, or if not a *Tycho-2* star, another identifier (for M67 we have IDs from Eggen & Sandage 1964; Sanders 1977; Montgomery et al. 1993; Fan et al. 1996). The table then lists, in order, the right ascension and declination for each M67 star

Table 12
Derived Cluster Bulk Kinematics

Cluster	Members		Bulk $V_{r,3D}$	Bulk $V_{r,3D+RV}$	$\mu_{\alpha\,\cos\delta}$	μ_{δ}	$\mu_{l\cos b}$	μ_{b}
	3D	3D+RV	(km s^{-1})	(km s^{-1})	(mas yr^{-1})	(mas yr^{-1})	(mas yr^{-1})	(mas yr^{-1})
Berkeley 86	2	...	−25.54 ± 2.60	...	−3.80 ± 1.27	−4.58 ± 1.24	−5.88 ± 1.25	0.90 ± 1.26
Collinder 205	1	6	27.40 ± 4.07	28.18 ± 1.52	−4.00 ± 2.10	8.00 ± 1.90	−8.08 ± 1.90	−3.84 ± 2.10
Collinder 258	2	6	16.04 ± 0.60	14.90 ± 0.93	−0.90 ± 2.62	−5.00 ± 2.40	0.35 ± 2.61	−5.07 ± 2.41
Harvard 10	3	...	−18.17 ± 1.94	...	−3.88 ± 1.07	−11.64 ± 1.11	−11.99 ± 1.11	2.58 ± 1.07
IC 2488	3	...	−1.84 ± 1.52	...	−7.73 ± 1.56	8.93 ± 1.50	−9.84 ± 1.50	−6.55 ± 1.56
IC 4651	9	10	−33.34 ± 0.67	−33.30 ± 0.67	−1.72 ± 0.70	−2.76 ± 0.69	−2.54 ± 0.69	2.04 ± 0.70
IC 4756	7	13	−24.44 ± 0.75	−25.08 ± 0.64	0.68 ± 0.74	−1.99 ± 0.72	−1.95 ± 0.72	−0.76 ± 0.74
Kharchenko 1	3	...	12.74 ± 1.31	...	6.10 ± 1.23	−1.91 ± 1.29	3.54 ± 1.29	5.32 ± 1.23
Lynga 1	1	6	−25.08 ± 4.33	−24.31 ± 0.52	−5.20 ± 4.50	−7.70 ± 4.10	−8.78 ± 4.36	−3.03 ± 4.25
Lynga 2	4	6	−9.64 ± 1.29	−9.94 ± 0.60	−3.88 ± 1.53	−8.61 ± 1.50	−8.99 ± 1.51	−2.89 ± 1.52
NGC 129	3	...	−39.41 ± 0.54	...	−2.37 ± 1.25	−1.32 ± 1.25	−2.46 ± 1.25	−1.15 ± 1.25
NGC 381	2	...	−29.76 ± 1.32	...	0.63 ± 2.87	−2.14 ± 2.96	0.75 ± 2.87	−2.10 ± 2.96
NGC 457	2	...	−32.99 ± 0.60	...	−2.84 ± 1.36	−0.04 ± 1.35	−2.82 ± 1.36	−0.31 ± 1.35
NGC 884	3	...	−19.35 ± 1.16	...	−0.64 ± 1.02	0.67 ± 1.01	−0.81 ± 1.02	0.44 ± 1.01
NGC 957	2	...	−34.34 ± 1.20	...	0.16 ± 1.35	−1.15 ± 1.45	0.54 ± 1.36	−1.03 ± 1.44
NGC 1513[a]	1	...	−15.13 ± 1.04	...	0.10 ± 2.70	−5.40 ± 2.60	3.60 ± 2.66	−4.02 ± 2.64
NGC 1528	5	...	−16.90 ± 0.48	...	1.29 ± 0.82	−0.94 ± 0.84	1.58 ± 0.83	0.14 ± 0.83
NGC 1662	6	20	−12.16 ± 1.35	−11.95 ± 0.86	−1.54 ± 0.73	−2.17 ± 0.73	1.77 ± 0.73	−1.98 ± 0.73
NGC 1960	8	...	−17.83 ± 0.99	...	0.50 ± 0.51	−4.50 ± 0.55	4.25 ± 0.54	−1.55 ± 0.52
NGC 2099	3	...	8.51 ± 0.92	...	4.53 ± 1.17	−7.43 ± 1.21	8.61 ± 1.20	1.25 ± 1.18
NGC 2215	3	4	−10.98 ± 0.68	−10.74 ± 0.66	5.07 ± 1.29	−6.35 ± 1.35	5.91 ± 1.35	5.58 ± 1.29
NGC 2264	1	9	24.06 ± 2.91	24.69 ± 0.98	−0.40 ± 2.00	−1.20 ± 2.00	1.16 ± 2.00	−0.51 ± 2.00
NGC 2301	2	...	8.25 ± 1.14	...	−0.55 ± 1.13	−6.20 ± 1.13	6.20 ± 1.13	−0.58 ± 1.13
NGC 2323	5	6	14.65 ± 1.32	14.70 ± 1.29	1.50 ± 0.93	−3.93 ± 0.99	3.82 ± 0.99	1.76 ± 0.93
NGC 2353	3	7	20.16 ± 0.61	18.78 ± 1.44	−2.75 ± 0.90	−2.18 ± 0.89	2.37 ± 0.89	−2.58 ± 0.90
NGC 2354	6	7	32.89 ± 0.39	32.86 ± 0.38	−9.27 ± 1.25	−2.13 ± 1.12	3.74 ± 1.12	−8.74 ± 1.25
NGC 2423	20	...	22.48 ± 0.94	...	−0.67 ± 0.39	−3.04 ± 0.39	3.08 ± 0.39	−0.43 ± 0.39
NGC 2437	18	19	46.99 ± 1.03	46.92 ± 1.03	−4.75 ± 0.47	0.09 ± 0.47	0.27 ± 0.47	−4.75 ± 0.47
NGC 2447	13	...	22.38 ± 0.20	...	−5.23 ± 0.61	4.33 ± 0.58	−3.69 ± 0.58	−5.70 ± 0.61
NGC 2482	4	...	34.88 ± 1.31	...	−2.05 ± 0.92	4.49 ± 0.85	−4.26 ± 0.85	−2.49 ± 0.92
NGC 2516	5	57	23.80 ± 0.71	23.32 ± 0.26	−4.20 ± 0.59	9.68 ± 0.59	−8.64 ± 0.59	−6.07 ± 0.59
NGC 2527	5	10	38.73 ± 0.56	39.17 ± 0.67	−3.92 ± 1.40	6.55 ± 1.23	−6.14 ± 1.23	−4.54 ± 1.40
NGC 2539	6	8	28.36 ± 0.41	28.34 ± 0.39	−3.82 ± 0.85	−3.35 ± 0.82	3.51 ± 0.82	−3.68 ± 0.85
NGC 2546	7	9	18.74 ± 0.57	21.12 ± 1.32	−3.77 ± 0.78	3.74 ± 0.72	−3.31 ± 0.72	−4.15 ± 0.78
NGC 2547	3	6	14.22 ± 1.28	15.65 ± 1.26	−6.74 ± 0.73	3.54 ± 0.72	−2.57 ± 0.72	−7.17 ± 0.73
NGC 2548	10	...	8.39 ± 0.34	...	0.61 ± 0.48	1.43 ± 0.50	−1.44 ± 0.50	0.59 ± 0.48
NGC 2567	3	6	35.63 ± 0.67	36.23 ± 0.74	−3.83 ± 1.90	1.78 ± 1.69	−1.48 ± 1.69	−3.96 ± 1.90
NGC 2579	2	5	1.50 ± 0.44	1.65 ± 0.38	−2.47 ± 1.42	1.44 ± 1.39	−1.23 ± 1.39	−2.58 ± 1.42
NGC 2669	1	7	20.56 ± 0.62	20.92 ± 0.48	−3.30 ± 1.30	6.20 ± 1.30	−6.10 ± 1.30	−3.48 ± 1.30
NGC 2670	1	7	15.74 ± 3.44	17.20 ± 0.83	−6.10 ± 2.10	4.80 ± 2.00	−4.62 ± 2.00	−6.24 ± 2.10
NGC 2682	10	33	33.67 ± 0.42	33.84 ± 0.33	−7.87 ± 0.61	−5.60 ± 0.59	5.57 ± 0.59	−7.88 ± 0.61
NGC 2925	2	...	−0.25 ± 2.14	...	−12.79 ± 1.55	3.60 ± 1.45	−5.38 ± 1.45	−12.15 ± 1.55
NGC 3680	10	11	1.06 ± 0.36	1.04 ± 0.35	−5.75 ± 0.61	1.15 ± 0.57	−4.45 ± 0.59	−3.81 ± 0.60
NGC 5281	2	6	−19.62 ± 0.57	−18.52 ± 0.75	−9.35 ± 1.67	−0.35 ± 1.59	−8.25 ± 1.65	4.40 ± 1.61
NGC 5316	8	...	−13.55 ± 0.48	...	−5.27 ± 1.06	−0.79 ± 1.00	−4.80 ± 1.04	2.30 ± 1.02
NGC 5460	5	...	−8.63 ± 2.00	...	−5.91 ± 0.56	−2.01 ± 0.59	−5.59 ± 0.58	2.78 ± 0.58
NGC 5617	3	6	−35.95 ± 0.80	−36.60 ± 0.86	1.15 ± 2.96	1.79 ± 2.74	2.11 ± 2.83	0.27 ± 2.87
NGC 5662	2	...	−14.46 ± 2.84	...	−2.20 ± 1.72	−4.77 ± 1.62	−5.15 ± 1.66	−1.05 ± 1.69
NGC 5822	13	...	−29.46 ± 0.49	...	−8.57 ± 0.95	−8.85 ± 0.88	−11.69 ± 0.89	3.88 ± 0.94
NGC 5823	2	8	−30.09 ± 3.23	−30.05 ± 0.79	−4.69 ± 3.24	−0.60 ± 2.98	−2.57 ± 3.03	3.97 ± 3.19
NGC 6025	6	...	16.10 ± 0.97	...	−1.92 ± 0.94	−2.42 ± 0.93	−2.73 ± 0.93	1.45 ± 0.94
NGC 6031	2	4	−6.23 ± 1.76	−2.48 ± 1.34	−1.65 ± 2.38	−9.92 ± 2.21	−10.05 ± 2.21	0.13 ± 2.38
NGC 6067	4	...	−39.83 ± 0.42	...	−2.69 ± 1.10	−1.76 ± 1.10	−2.09 ± 1.10	2.44 ± 1.10
NGC 6124	10	11	−19.89 ± 0.99	−19.87 ± 0.98	−0.07 ± 0.51	−3.42 ± 0.52	−3.42 ± 0.52	−0.16 ± 0.51
NGC 6134	7	9	−27.30 ± 0.67	−27.41 ± 0.59	−0.11 ± 1.12	−6.97 ± 1.09	−6.96 ± 1.09	−0.38 ± 1.12
NGC 6167	3	5	−20.53 ± 0.73	−21.32 ± 0.41	−1.94 ± 1.35	−1.55 ± 1.31	−1.63 ± 1.31	1.86 ± 1.35
NGC 6250	1	5	−7.98 ± 0.99	−8.04 ± 0.81	13.50 ± 1.70	−11.20 ± 1.70	−11.60 ± 1.70	−13.15 ± 1.70
NGC 6281	6	11	−6.33 ± 0.74	−6.36 ± 0.60	−2.86 ± 0.75	−3.66 ± 0.76	−3.54 ± 0.76	3.01 ± 0.75
NGC 6405	6	10	−8.27 ± 0.45	−7.02 ± 1.53	−1.49 ± 0.63	−6.10 ± 0.64	−5.89 ± 0.64	2.18 ± 0.63
NGC 6416	6	10	−27.02 ± 1.58	−27.52 ± 0.94	−0.36 ± 0.91	−0.14 ± 0.99	−0.09 ± 0.99	0.37 ± 0.91
NGC 6603	2	4	21.33 ± 0.96	21.34 ± 0.92	0.98 ± 1.06	0.51 ± 1.15	0.39 ± 1.15	−1.03 ± 1.06
NGC 6705	4	6	30.48 ± 1.42	30.87 ± 1.14	−5.38 ± 1.19	−0.35 ± 1.25	−0.05 ± 1.25	5.39 ± 1.19
NGC 6811	7	...	6.03 ± 0.30	...	−5.31 ± 0.67	−8.13 ± 0.64	−9.67 ± 0.65	0.92 ± 0.66
NGC 6866	2	...	12.18 ± 0.75	...	−5.52 ± 1.17	−7.97 ± 1.09	−9.67 ± 1.11	0.61 ± 1.15
NGC 6885	2	6	−1.60 ± 0.99	−1.50 ± 0.87	−2.90 ± 1.41	−6.05 ± 1.34	−6.70 ± 1.35	0.41 ± 1.40

Table 12
(Continued)

Cluster	Members		Bulk $V_{r,3D}$	Bulk $V_{r,3D+RV}$	$\mu_{\alpha\cos\delta}$	μ_δ	$\mu_{l\cos b}$	μ_b
	3D	3D+RV	(km s^{-1})	(km s^{-1})	(mas yr^{-1})	(mas yr^{-1})	(mas yr^{-1})	(mas yr^{-1})
NGC 7209	6	...	−20.50 ± 0.67	...	1.81 ± 0.69	−0.04 ± 0.66	1.44 ± 0.68	−1.09 ± 0.67
NGC 7654[a]	1	...	−57.39 ± 2.14	...	0.40 ± 5.00	0.60 ± 5.20	0.55 ± 5.02	0.46 ± 5.18
Platais 1	3	...	−26.73 ± 0.40	...	−4.50 ± 1.09	−3.78 ± 1.08	−5.88 ± 1.09	0.16 ± 1.08
Ruprecht 119	3	6	−12.77 ± 1.34	−11.21 ± 1.34	0.92 ± 1.46	−1.25 ± 1.44	−1.18 ± 1.44	−1.00 ± 1.46
Stock 8	3	...	−18.01 ± 1.50	...	−1.81 ± 1.06	−4.23 ± 1.07	2.90 ± 1.07	−3.57 ± 1.06
Trumpler 10	2	8	27.62 ± 3.10	32.17 ± 0.76	−12.17 ± 0.81	8.05 ± 0.78	−7.81 ± 0.78	−12.33 ± 0.81

Note. [a] Bulk cluster parameters unreliable due to membership uncertainty.

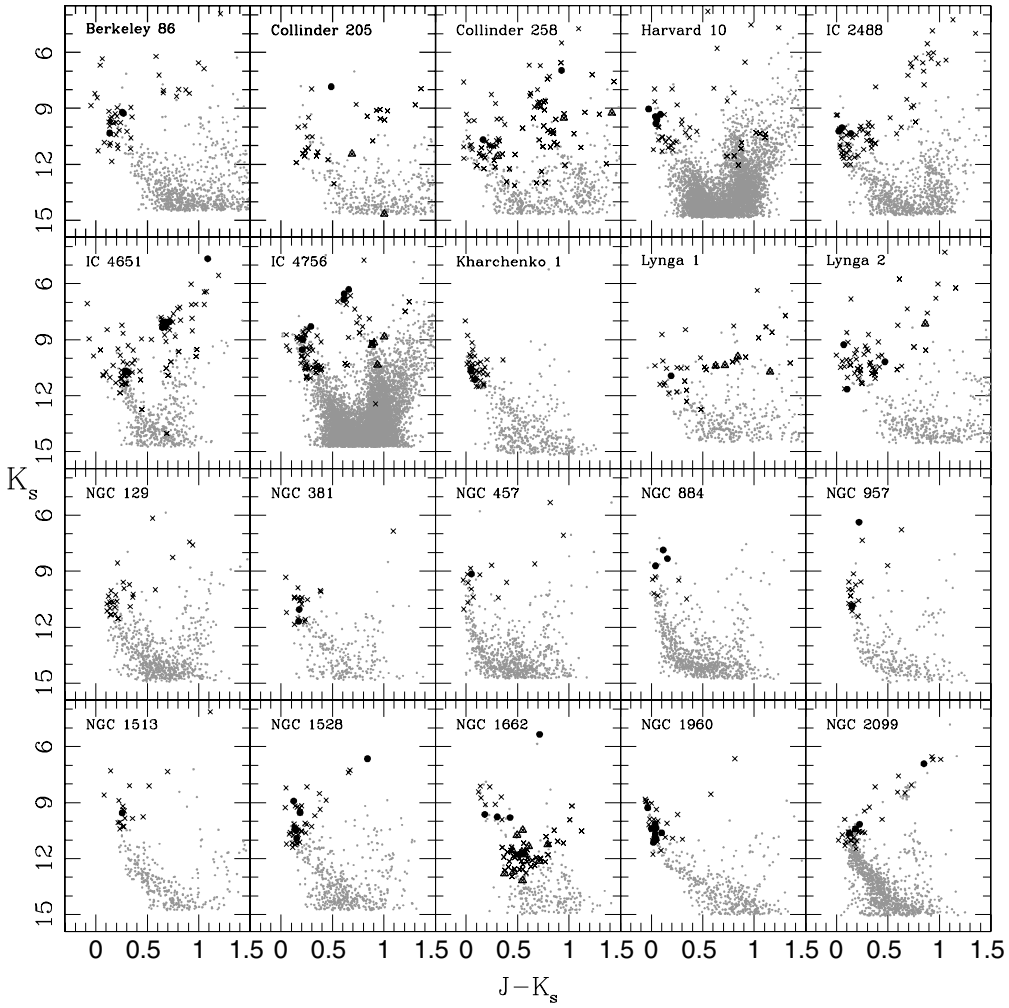

Figure 12. 2MASS CMD for all clusters using stars inside the cluster radius (Dias et al. 2002b). Crosses (×) denote stars with proper motion data that we determined to be non-members. Large circles denote stars selected to be members based on *both* RV and proper motion criteria. Triangles denote stars that have $P_c^V > 70\%$ but which do not have *Tycho-2* proper motion data available.

(Columns 2 and 3), the *Tycho-2* proper motions and errors (Columns 4–7), our measured RV and error (Columns 8 and 9), and which spectral cross-correlation template was used to derive these (Column 10). In addition, we have included the membership probability from Dias et al. (2001, 2002a; Column 11) for comparison to our derived membership probabilities $P_c^K \times 100$ (PM; Column 12), $P_c^V \times 100$ (RV; Column 13), and $P_c^{\rm tot}$, the joint probability ($P_c^{\rm tot} = P_c^V P_c^K \times 100$; Column 14). The stars selected as cluster members are presented in boldface type.

Similar probability data are given for the other clusters in our sample in Table 10, which is available in an electronic format. In this table we give for each star observed its *Tycho-2* name, or, if a non-Tycho star, an identifier with the format "XXXX_f_####" for the added "filler" candidate FOPS guide stars or "XXXX_u_####," for USNO B-1.0 catalog "filler" stars, categories described in the observational criteria in Section 2.2. In Section 6.2.3 our analysis of the cluster memberships of these stars are compared against the membership analysis by Dias et al. (2001), whose membership probabilities are based only on proper motion.

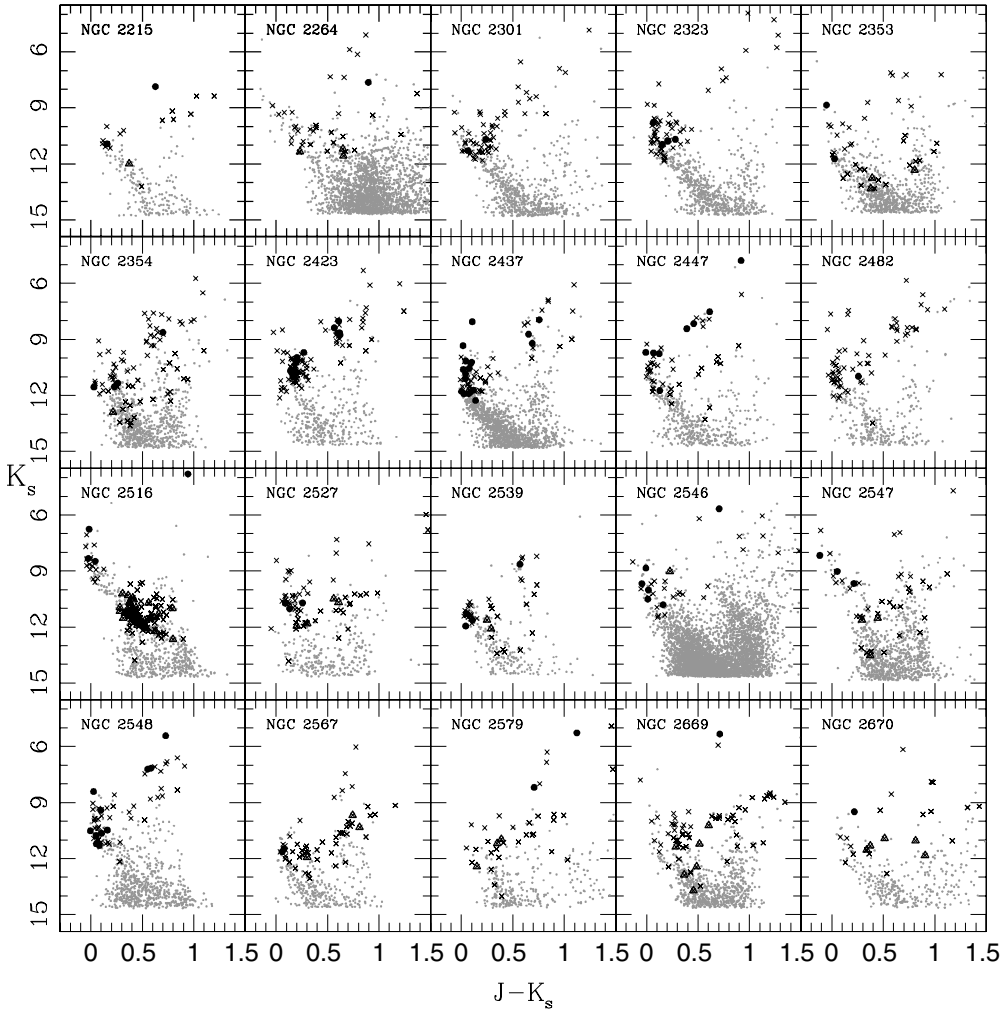

Figure 13. Continuation of Figure 12.

5.6. Cluster Membership and Cluster CMDs

As shown in Figure 1, with only photometric data the identification of open cluster sequences in the CMD can often be a tricky prospect. Our radial velocity cluster memberships can significantly aid in clarifying the location of these cluster sequences. The 2MASS and *Tycho-2* photometry for all stars in our survey with measured RVs are listed in Table 11.

Figure 11 shows the 2MASS CMD for the example cluster NGC 2682 with our spectroscopically-observed stars identified, and with large circles denoting stars selected to be members based on *both* RV and proper motion. Triangles denote stars that have $P_c^V \geqslant 70\%$ but which do not have *Tycho-2* proper motion data. For now we present CMDs without reddening corrections applied, because this is a non-trivial process in that not all line-of-sight reddening (the values typically given in catalogs such as Schlegel et al. 1998) is necessarily foreground to the cluster. One can see from the CMD that in this case our membership census yields members that fall primarily along the photometric sequences of M67 apparent in the CMD. Similar 2MASS CMD membership plots for all clusters we have studied are shown in Figures 12–15. As in the case of M67, our identified members typically fall in the expected locations of the main sequence turn-off (MSTO) or giant branches of the clusters, when those are obvious; however, in many cases the CMDs are crowded with field star contamination and our identified members help clarify the cluster sequences. This is particularly useful in the fairly common situation where the giant branches are sparsely populated. As we shall show in another contribution (P. M. Frinchaboy et al. 2008, in preparation), our ability to clarify the CMD locations of cluster giant branches and MSTOs greatly improves the isochrone fitting for these systems.

6. KINEMATICAL RESULTS

6.1. Derived Cluster Space Velocities

The cluster bulk RV is calculated using cluster members (e.g., as shown in Table 9) and techniques from Pryor & Meylan (1993) to determine the cluster mean RV and error in the mean. The cluster mean bulk proper motions are calculated using the following equations (and a symmetrical version for μ_δ):

$$\langle \mu_{\alpha\cos(\delta)} \rangle = \frac{\sum_{i=1}^{n} \left(\frac{\mu_{i,\alpha\cos(\delta)}}{\sigma^2_{\mu_{\alpha\cos(\delta)},i}} \right)}{\sum_{i=1}^{n} \left(\frac{1}{\sigma^2_{\mu_{\alpha\cos(\delta)},i}} \right)} \quad (6)$$

$$\epsilon_{\mu_{\alpha\cos(\delta)}} = \frac{1}{\sum_{i=1}^{n} \left(\frac{1}{\sigma^2_{\mu_{\alpha\cos(\delta)},i}} \right)}. \quad (7)$$

The derived cluster bulk motions are given in Table 12, where we list the numbers of members with full space motions

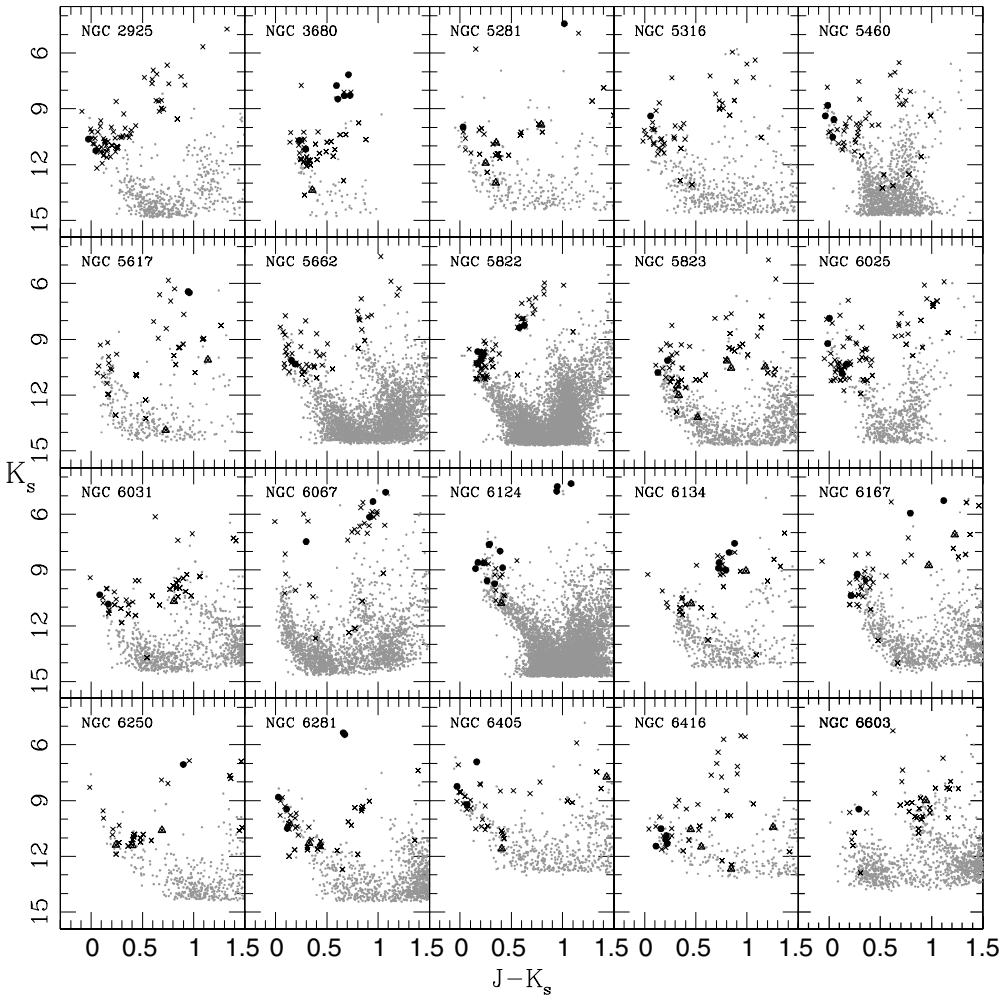

Figure 14. Continuation of Figure 12.

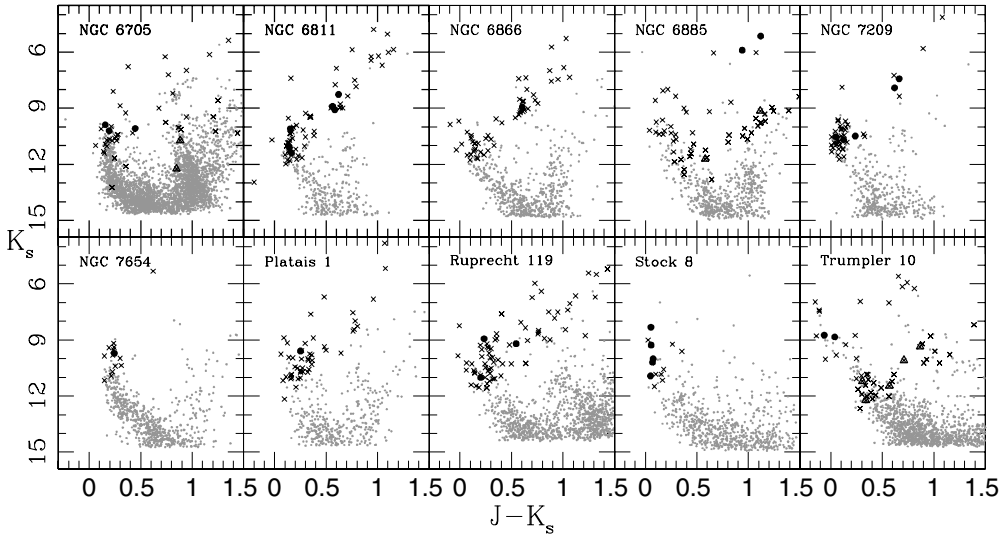

Figure 15. Continuation of Figure 12.

(Column 2) and the 3D members plus the stars determined to be members by RV criteria alone (3D+RV; Column 3), along with the resulting bulk kinematics and the associated uncertainties (RV from all 3D members; Column 4), RV from 3D *and* additional "RV only" members (Column 5), and equatorial and Galactic system proper motions (Columns 6–9). We find two clusters NGC 1513 and NGC 7654 with only one star selected for membership (i.e., the membership method found no more than one star with a given RV within the errors); given the uncertainty in selecting among single star subsamples to define the actual "cluster," we remove these two clusters from further analysis.

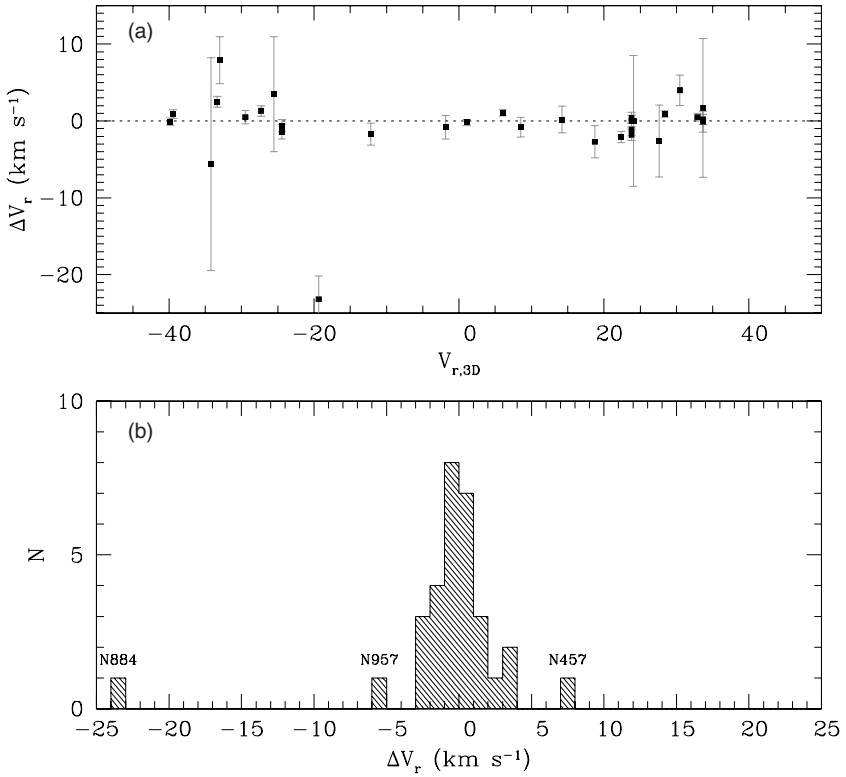

Figure 16. Comparison of radial velocities ΔV_r to previous studies (see Table 14). (a) ΔV_r plotted as a function of our measured V_r; no obvious systematic trend is seen. (b) Histogram of ΔV_r showing that, besides the cases of NGC 457, NGC 884, and NGC 957 which all compared here to the results by Liu et al. (1989, see Section 6.2.2), all of our measurements of the bulk RVs of the clusters are within 5 km s^{-1} of all previous determined cluster measurements, and with the peak at $\Delta V_r = 0$ km s^{-1}.

Table 13
Derived NGC 2682 Motions Compared to Previous Results

Parameter	Units	$N_{members}$	Value	References
$\mu_\alpha \cos\delta$	(mas yr^{-1})	10	-7.87 ± 0.61	This Work
	(mas yr^{-1})	30	-8.62 ± 0.28	Dias et al. (2001)
	(mas yr^{-1})	27	-8.31 ± 0.26	Kharchenko et al. (2005)
μ_δ	(mas yr^{-1})	10	-5.60 ± 0.59	This Work
	(mas yr^{-1})	30	-6.00 ± 0.28	Dias et al. (2001)
	(mas yr^{-1})	27	-4.81 ± 0.22	Kharchenko et al. (2005)
V_r	(km s^{-1})	10	33.67 ± 0.42	This Work
	(km s^{-1})	13	32 ± 9	Scott et al. (1995)
	(km s^{-1})	104	33.5 ± 0.5	Mathieu et al. (1986)

6.2. Comparison with Previous Results

6.2.1. NGC2682 (M67) Example

In Section 3.7 and Table 6 we have already demonstrated a star-by-star comparison of derived RVs for the example cluster M67. For stars in common between the surveys, we find excellent agreement in the determined per star RVs (previously shown in Figure 7). Now we compare the derived bulk space velocity for this very well-studied cluster with the most detailed, previous studies of M67.

In Table 13 we compare our derived mean proper motion and radial velocity for M67, averaged over these measured parameters for ten stars we determined to be reliable 3D members of the cluster, against derivations of these bulk motion parameters by other authors. With regard to the previously derived bulk RV for M67, our mean radial velocity is consistent with previous measurements by Mathieu et al. (1986) and Scott et al. (1995), and lies within 0.2 km s^{-1} of the rather precise value given in the Mathieu et al. study. The total number of published clusters having as extensive and detailed RV coverage as the Mathieu et al. M67 study is less than ten, whereas our study now provides high-precision RVs for stars in nearly five times as many clusters. We also find proper motion results more or less consistent with previous measured values, with our μ_δ value being bracketed by the μ_δ measurements by Dias et al. (2001) and Kharchenko et al. (2005) results and our $\mu_\alpha \cos\delta$ reasonably close to the values for this proper motion component derived by these two other studies. The previous studies have smaller errors in their mean due to the larger numbers of "member" stars used in the determination of the bulk proper motion.

Thus we find that our survey results are consistent with the very detailed analysis of previous M67 work. Despite the fact that M67 is probably one of the most well-studied open clusters in the Galaxy and previous studies typically utilized many more stars than we have, our results deliver comparable precision to the best of these because of the greater purity of our samples, and, in the case of the RV measurement, the velocity resolution of our spectra.

6.2.2. Comparison to Previously Derived Bulk Cluster Radial Velocities

A compilation of our derived mean cluster RVs compared to those found previously by other authors is given in Table 14. We have found previous results for 25 of our 71 studied clusters, some with multiple studies. In general, we find consistency with the previous studies to the few km s^{-1} level, as shown in Figure 16, but in a few cases, there are more substantial differences.

Table 14
Comparison of Derived Cluster RVs

Cluster	Members		Bulk $V_{r,3D}$	Bulk $V_{r,3D+RV}$	Other V_r	#	$\Delta V_{r,3D}$	$\Delta V_{r,3D+RV}$	Reference
	3D	3D+RV	(km s^{-1})	(km s^{-1})	(km s^{-1})	stars	(km s^{-1})	(km s^{-1})	
Berkeley 86	2	...	−25.54 ± 2.64	...	−22.0 ± 7.0	6	+3.5	...	Forbes et al. (1992)
IC 2488	3	...	−1.84 ± 1.52	...	−2.6 ± 0.1	...	−0.8	...	Claria et al. (2003)
IC 4651	9	10	−33.34 ± 0.67	−33.30 ± 0.67	−31.0 ± 0.2	14	+2.3	+2.3	Mermilliod et al. (1995)
					−30.8 ± 0.3	44	+2.5	+2.5	Meibom et al. (2002)
IC 4756	7	13	−24.44 ± 0.75	−25.08 ± 0.64	−25.8 ± 0.6	13	−1.4	−0.7	Mermilliod & Mayor (1990)
					−25.0 ± 0.2	15	−0.6	+0.1	Valitova et al. (1990)
NGC 129	3	...	−39.41 ± 0.54	...	−38.5 ± 0.2	2	+0.9	...	Mermilliod et al. (1987)
NGC 457	2	...	−32.99 ± 0.60	...	−25.1 ± 3.0	4	+7.9	...	Liu et al. (1989)
NGC 884	3	...	−19.35 ± 1.16	...	−42.5 ± 2.8	2	−23.2	...	Liu et al. (1989)
NGC 957	2	...	−34.21 ± 1.22	...	−28.6 ± 13.8	2	−5.6	...	Liu et al. (1989)
NGC 1662	6	20	−12.16 ± 1.35	−11.95 ± 0.86	−13.9 ± 0.5	...	−1.7	−2.0	Grenier et al. (1999)
NGC 2099	3	...	+8.51 ± 0.92	...	+7.7 ± 0.9	30	−0.8	...	Mermilliod et al. (1996)
NGC 2264	1	9	+24.06 ± 2.91	+24.71 ± 0.95	+24.1 ± 8.0	6	+0.0	−0.6	Liu et al. (1989)
NGC 2354	6	7	+32.89 ± 0.39	+32.86 ± 0.38	+33.4 ± 0.3	...	+0.5	+0.5	Claria et al. (1999)
NGC 2447	13	...	+22.38 ± 0.20	...	+21.7 ± 0.7	11	−2.1	...	Mermilliod & Mayor (1989)
NGC 2516	5	57	+23.80 ± 0.71	+23.32 ± 0.26	+22.7 ± 0.4	...	−1.1	+0.6	Robichon et al. (1999)
					+24.2 ± 0.2	57	+0.4	+0.9	Terndrup et al. (2002)
					+23.8 ± 0.3	24	+0.0	+0.5	Jeffries et al. (1998)
					+22.0 ± 0.2	22	−1.8	−1.3	Gonzalez & Lapasset (2001)
NGC 2539	6	8	+28.36 ± 0.41	+28.34 ± 0.39	+29.3 ± 0.1	09	+0.9	+1.0	Mermilliod & Mayor (1989)
NGC 2546	7	9	+18.74 ± 0.57	+21.12 ± 1.32	+16.0 ± 2.0	...	−2.7	−5.1	Hron (1987)
NGC 2547	3	6	+14.22 ± 1.28	+15.65 ± 1.26	+14.4 ± 1.2	...	+0.2	−1.3	Robichon et al. (1999)
NGC 2682	10	33	+33.67 ± 0.42	+33.84 ± 0.33	+33.5 ± 0.5	104	+0.2	+0.3	Mathieu et al. (1986)
					+33.8 ± 1.3	04	−0.1	+0.0	Prichet & Glaspey (1991)
					+32.0 ± 9.0	33	+1.7	+1.8	Scott et al. (1995)
NGC 3680	10	11	+1.06 ± 0.36	+1.04 ± 0.35	+0.9 ± 0.2	6	−0.2	−0.2	Mermilliod et al. (1995)
NGC 5822	13	...	−29.46 ± 0.49	...	−29.0 ± 0.7	...	+0.5	...	Mermilliod & Mayor (1990)
NGC 6067	4	...	−39.83 ± 0.42	...	−39.9 ± 0.2	10	−0.1	...	Mermilliod et al. (1987)
NGC 6134	7	9	−27.30 ± 0.67	−27.41 ± 0.59	−26.0 ± 0.2	14	+1.3	+1.4	Claria & Mermilliod (1992)
NGC 6705	4	6	+30.48 ± 1.42	+30.87 ± 1.14	+34.5 ± 1.4	29	+4.0	+3.6	Mathieu et al. (1986)
NGC 6811	7	...	+6.03 ± 0.30	...	+7.1 ± 0.3	03	+1.1	...	Mermilliod & Mayor (1990)
Trumpler 10	2	8	+27.62 ± 3.10	+31.91 ± 0.73	+25.0 ± 3.5	22	−2.6	−6.9	Robichon et al. (1999)

Figure 16 shows that the clusters NGC 457, NGC 884, and NGC 957 have discrepant RVs found between our work and any previous study; however all of these clusters, plus NGC 2264, were studied by Liu et al. (1989). The Liu et al. (1989) study is comprised of only a few possible cluster members observed (e.g., for NGC 884 and NGC 957 only two stars each and these clusters also have large mean errors). We believe our results, which incorporate both RV and proper motion membership, are superior to those from Liu et al. (1989). Even with the small numbers of stars in both studies, we find that our results are marginally consistent with Liu et al. (1989) for NGC 2264.

6.2.3. Comparison to Previously Derived Bulk Cluster Proper Motions

In Table 15, we compare our derived open cluster bulk proper motions with the previous results of Dias et al. (2001, 2002a). The latter surveys used only the *Tycho-2* proper motions to derive membership and the cluster bulk proper motions. Table 15 compares the numbers of stars used by Dias et al. and their derived mean cluster proper motions (Columns 2–5) to our own sample statistics and derived mean proper motions (Columns 6–9). As shown in Figure 17 (gray histogram), three clusters—Collinder 258, Lynga 1, and NGC 6250—show large inconsistencies ($\Delta\mu > 5$ mas yr^{-1}) between our results and those of Dias et al. We also remind the reader that we have already excluded two other cases (NGC 1513 and NGC 7654; see Section 6.1) from our study, because we identified only one star selected as a possible cluster member. Looking further at the proper motion difference outliers, we find that each Lynga 1 and NGC 6250 have only one star with fully derived 3D kinematics and in the case of Collinder 258 there are only two member stars. Thus, we conclude that our analysis may have settled on the wrong star(s) to represent the cluster in these cases and that the results for Collinder 258, Lynga 1, and NGC 6250 (in addition to NGC 1513 and NGC 7654) may not be reliable. For the remaining 66 of our 71 clusters, our "re-measured" proper motions are within the 1σ errors of those found by Dias et al. (2001, 2002a), though our data generally have comparable or smaller resulting errors in the mean (as shown in Figure 17) of $\sim$1.5 mas yr^{-1}.

The direct comparison to the Dias et al. proper motions is shown in Figure 17, with the full sample shown in gray and various subsamples based on the number of members in either survey shown by the colored histograms. A somewhat close agreement with Dias et al. is expected because we are deriving proper motions using a subsample of Dias et al. stars and adopting the same astrometry. A key difference, however, is that a number of Dias et al. "member" stars are excluded by our RV membership criterion so that, while we typically derive approximately the same bulk motions as Dias et al., these authors allow many more actual non-members to enter their sample; nevertheless, that Dias et al. include more actual non-members seems to have relatively small effects because these authors are typically averaging over a large number of stars in

Table 15
Comparison of Derived Mean Proper Motions to those of Dias et al. (2001, 2002a)

Cluster	Dias et al. (2001, 2002a)				This study			Comparison			
	Stars	Memb.	$\mu_{\alpha\cos\delta}$ (mas yr^{-1})	μ_δ (mas yr^{-1})	Memb	$\mu_{\alpha\cos\delta}$ (mas yr^{-1})	μ_δ (mas yr^{-1})	$\Delta\mu_{\alpha\cos\delta}$ (mas yr^{-1})	$\Delta\mu_\delta$ (mas yr^{-1})	Dias Memb. Conf.	Dias Memb. Rej.
Berkeley 86	99	50	−4.1 ± 2.2	−4.5 ± 2.2	2	−3.8 ± 1.3	−4.6 ± 1.2	−0.3	0.1	2	22
Collinder 205	19	12	−3.9 ± 1.9	6.5 ± 1.9	1	−4.0 ± 2.1	8.0 ± 1.9	0.1	−1.5	1	4
Collinder 258[a]	25	13	−8.1 ± 2.2	−0.8 ± 2.2	2	−0.9 ± 2.6	−5.0 ± 2.4	−7.2	4.2	0	8
Harvard 10	92	34	−2.8 ± 1.6	−11.2 ± 1.6	3	−3.9 ± 1.1	−11.6 ± 1.1	1.1	0.4	3	11
IC 2488	63	40	−5.6 ± 3.0	8.0 ± 3.0	3	−7.7 ± 1.6	8.9 ± 1.5	2.1	−0.9	3	22
IC 4651	43	19	−1.1 ± 2.1	−2.2 ± 2.1	9	−1.7 ± 0.7	−2.8 ± 0.7	0.6	0.6	7	16
IC 4756	181	30	−0.1 ± 1.3	−3.4 ± 1.3	7	0.7 ± 0.7	−2.0 ± 0.7	−0.8	−1.4	4	8
Kharchenko 1	86	40	2.1 ± 3.6	−3.5 ± 3.6	3	6.1 ± 1.2	−1.9 ± 1.3	−4.0	−1.6	3	14
Lynga 1[a]	23	9	−7.7 ± 2.9	−2.4 ± 2.9	1	−5.2 ± 4.5	−7.7 ± 4.1	−2.5	5.3	1	11
Lynga 2	33	13	−5.2 ± 3.2	−5.9 ± 3.2	4	−3.9 ± 1.5	−8.6 ± 1.5	−1.3	2.7	2	4
NGC 129	39	10	−1.1 ± 2.8	1.6 ± 2.8	3	−2.4 ± 1.2	−1.3 ± 1.2	1.3	2.9	3	17
NGC 381	25	13	0.9 ± 1.9	−1.3 ± 1.9	2	0.6 ± 2.9	−2.1 ± 3.0	0.3	0.8	2	9
NGC 457	29	14	−0.6 ± 2.5	−1.9 ± 2.5	2	−2.8 ± 1.4	0.0 ± 1.4	2.2	−1.9	2	9
NGC 884	46	18	−1.6 ± 2.5	0.2 ± 2.5	3	−0.6 ± 1.0	0.7 ± 1.0	−1.0	−0.5	3	12
NGC 957	28	12	1.1 ± 3.5	0.3 ± 3.5	2	0.2 ± 1.4	−1.1 ± 1.4	0.9	1.4	2	11
NGC 1513	20	6	5.0 ± 3.8	−3.6 ± 3.8	1	0.1 ± 2.7	−5.4 ± 2.6	4.9	1.8	1	8
NGC 1528	63	20	1.4 ± 1.7	−1.5 ± 1.7	5	1.3 ± 0.8	−0.9 ± 0.8	0.1	−0.6	5	14
NGC 1662	34	18	−1.9 ± 1.2	−2.2 ± 1.2	6	−1.5 ± 0.7	−2.2 ± 0.7	−0.4	0.0	6	5
NGC 1960	49	30	0.1 ± 1.6	−4.0 ± 1.6	18	0.5 ± 0.5	−4.5 ± 0.6	−0.4	0.5	8	18
NGC 2099	84	40	3.8 ± 1.8	−7.1 ± 1.8	3	4.5 ± 1.2	−7.4 ± 1.2	−0.7	0.3	3	23
NGC 2215	17	12	2.6 ± 1.9	−5.6 ± 1.9	3	5.1 ± 1.3	−6.3 ± 1.4	−2.5	0.7	3	8
NGC 2264	81	30	−1.1 ± 2.0	−3.8 ± 1.0	1	−0.4 ± 2.0	−1.2 ± 2.0	−0.7	−2.6	1	7
NGC 2301	89	45	−1.3 ± 1.8	−5.0 ± 1.8	2	−0.6 ± 1.1	−6.2 ± 1.1	−0.7	1.2	2	23
NGC 2323	100	55	0.6 ± 2.0	−1.9 ± 2.0	5	1.5 ± 0.9	−3.9 ± 1.0	−0.9	2.0	3	17
NGC 2353	35	25	−2.5 ± 2.6	0.0 ± 2.6	3	−2.8 ± 0.9	−2.2 ± 0.9	0.3	2.2	3	15
NGC 2354	69	20	−5.8 ± 2.9	−1.5 ± 2.9	6	−9.3 ± 1.2	−2.1 ± 1.1	3.5	0.6	6	19
NGC 2423	93	50	0.6 ± 1.9	−2.6 ± 1.9	20	−0.7 ± 0.4	−3.0 ± 0.4	1.3	0.4	18	22
NGC 2437	144	75	−4.5 ± 1.4	0.6 ± 1.4	18	−4.8 ± 0.5	0.1 ± 0.5	0.3	0.5	18	14
NGC 2447	69	34	−4.8 ± 1.9	4.4 ± 1.9	13	−5.2 ± 0.6	4.3 ± 0.6	0.4	0.1	13	14
NGC 2482	57	32	−4.9 ± 3.0	1.6 ± 3.0	4	−2.0 ± 0.9	4.5 ± 0.8	−2.9	−2.9	2	15
NGC 2516	81	45	−3.2 ± 1.7	10.1 ± 1.7	5	−4.2 ± 0.6	9.7 ± 0.6	1.0	0.4	5	8
NGC 2527	62	32	−4.1 ± 2.9	6.4 ± 2.9	5	−3.9 ± 1.4	6.5 ± 1.2	−0.2	−0.1	5	22
NGC 2539	50	30	−4.1 ± 1.4	−1.8 ± 1.4	6	−3.8 ± 0.8	−3.4 ± 0.8	−0.3	1.6	5	14
NGC 2546	286	80	−4.0 ± 2.2	3.6 ± 2.2	7	−3.8 ± 0.8	3.7 ± 0.7	−0.2	−0.1	7	21
NGC 2547	38	19	−7.7 ± 1.9	3.8 ± 1.9	3	−6.7 ± 0.7	3.5 ± 0.7	−1.0	0.3	3	7
NGC 2548	107	70	−0.8 ± 1.7	1.9 ± 1.7	10	0.6 ± 0.5	1.4 ± 0.5	−1.4	0.5	10	30
NGC 2567	30	17	−3.2 ± 2.6	2.3 ± 2.6	3	−3.8 ± 1.9	1.8 ± 1.7	0.6	0.5	3	8
NGC 2579	14	10	−4.1 ± 1.9	2.9 ± 1.9	2	−2.5 ± 1.4	1.4 ± 1.4	−1.6	1.5	2	5
NGC 2669	32	16	−5.8 ± 3.5	4.1 ± 3.5	1	−3.3 ± 1.3	6.2 ± 1.3	−2.5	−2.1	1	10
NGC 2670	18	9	−8.1 ± 2.2	5.9 ± 2.2	1	−6.1 ± 2.1	4.8 ± 2.0	−2.0	1.1	0	1
NGC 2682	53	30	−8.6 ± 1.5	−6.0 ± 1.5	10	−7.9 ± 0.6	−5.6 ± 0.6	−0.7	−0.4	10	9
NGC 2925	71	32	−8.9 ± 2.5	5.4 ± 2.5	2	−12.8 ± 1.6	3.6 ± 1.4	3.9	1.8	2	14
NGC 3680	24	14	−5.9 ± 2.2	2.0 ± 2.2	10	−5.8 ± 0.6	1.1 ± 0.6	−0.1	0.9	10	9
NGC 5281	29	12	−5.3 ± 2.6	−3.5 ± 2.6	2	−9.3 ± 1.7	−0.3 ± 1.6	4.0	−3.2	0	4
NGC 5316	97	25	−5.0 ± 2.3	0.2 ± 2.3	8	−5.3 ± 1.1	−0.8 ± 1.0	0.3	1.0	8	16
NGC 5460	94	40	−6.6 ± 2.7	−2.6 ± 2.7	5	−5.9 ± 0.6	−2.0 ± 0.6	−0.7	−0.6	5	22
NGC 5617	54	35	−2.0 ± 3.6	−2.3 ± 3.6	3	1.1 ± 3.0	1.8 ± 2.7	−3.1	−4.1	3	16
NGC 5662	109	60	−5.0 ± 2.9	−5.6 ± 2.9	2	−2.2 ± 1.7	−4.8 ± 1.6	−2.8	−0.8	2	26
NGC 5822	257	140	−8.0 ± 2.8	−8.2 ± 2.8	13	−8.6 ± 0.9	−8.8 ± 0.9	0.6	0.6	13	46
NGC 5823	31	10	−3.8 ± 1.9	0.1 ± 1.9	2	−4.7 ± 3.2	−0.6 ± 3.0	0.9	0.7	2	11
NGC 6025	66	30	−3.1 ± 2.0	−3.3 ± 2.0	6	−1.9 ± 0.9	−2.4 ± 0.9	−1.2	−0.9	5	15
NGC 6031	21	11	−2.4 ± 2.4	−7.5 ± 2.4	1	−1.7 ± 2.4	−9.9 ± 2.2	−0.7	2.4	2	6
NGC 6067	114	24	−1.7 ± 2.6	−2.5 ± 2.6	4	−2.7 ± 1.1	−1.8 ± 1.1	1.0	−0.7	4	8
NGC 6124	117	60	−1.3 ± 2.0	−3.1 ± 2.0	10	−0.1 ± 1.1	−3.4 ± 0.5	−1.2	0.3	10	36
NGC 6134	28	15	−0.9 ± 3.3	−4.6 ± 3.3	7	−0.1 ± 1.1	−7.0 ± 1.1	−0.8	2.4	3	3
NGC 6167	22	10	−1.4 ± 2.6	−5.5 ± 2.6	3	−1.9 ± 1.4	−1.6 ± 1.3	0.5	−3.9	0	0
NGC 6250[a]	23	10	−0.2 ± 1.6	−3.3 ± 1.6	1	13.5 ± 1.7	−11.2 ± 1.7	−13.7	7.9	0	3
NGC 6281	37	21	−3.4 ± 2.5	−3.6 ± 2.5	6	−2.9 ± 0.8	−3.7 ± 0.8	−0.5	0.1	6	10
NGC 6405	60	30	−2.2 ± 2.4	−5.4 ± 2.2	5	−1.5 ± 0.6	−6.1 ± 0.6	−0.7	0.6	6	12
NGC 6416	70	32	−1.4 ± 2.4	0.2 ± 2.4	6	−0.4 ± 0.9	−0.1 ± 1.0	−1.0	0.3	6	8
NGC 6603	44	22	0.7 ± 2.3	0.1 ± 2.3	3	1.0 ± 1.1	0.5 ± 1.2	−0.3	−0.4	2	6
NGC 6705	64	32	−4.6 ± 2.7	−1.1 ± 2.7	4	−5.4 ± 1.2	−0.3 ± 1.2	0.8	−0.8	4	12
NGC 6811	102	51	−5.5 ± 1.9	−7.5 ± 1.9	7	−5.3 ± 0.7	−8.1 ± 0.6	−0.2	0.6	7	26

Table 15
(Continued)

Cluster	Dias et al. (2001, 2002a)				This study			Comparison			
	Stars	Memb.	$\mu_{\alpha\cos\delta}$	μ_δ	Memb	$\mu_{\alpha\cos\delta}$	μ_δ	$\Delta\mu_{\alpha\cos\delta}$	$\Delta\mu_\delta$	Dias Memb.	
			(mas yr^{-1})	(mas yr^{-1})		(mas yr^{-1})	(mas yr^{-1})	(mas yr^{-1})	(mas yr^{-1})	Conf.	Rej.
NGC 6866	89	45	−3.4 ± 2.9	−5.0 ± 2.9	2	−5.5 ± 1.2	−8.0 ± 1.1	2.1	3.0	2	30
NGC 6885	46	20	−2.6 ± 2.6	−4.3 ± 2.6	2	−2.9 ± 1.4	−6.0 ± 1.3	0.3	1.7	2	10
NGC 7209	72	36	1.5 ± 1.9	1.4 ± 1.9	1	1.8 ± 0.7	−0.0 ± 0.6	−0.3	1.4	6	22
NGC 7654	25	10	−0.6 ± 2.7	0.9 ± 2.7	1	0.4 ± 5.0	0.6 ± 5.2	1.0	−0.3	1	8
Platais 1	59	25	−3.7 ± 2.9	−4.0 ± 2.9	3	−4.5 ± 1.1	−3.8 ± 1.1	0.8	−0.2	3	26
Ruprecht 119	31	14	−1.2 ± 1.5	−1.8 ± 1.5	3	0.9 ± 1.5	−1.2 ± 1.4	−2.1	−0.6	2	6
Stock 8	24	15	−1.0 ± 1.7	−5.4 ± 1.7	3	−1.8 ± 1.1	−4.2 ± 1.1	0.8	−1.2	3	7
Trumpler 10	44	22	−12.1 ± 1.5	6.7 ± 1.5	1	−12.2 ± 0.8	8.1 ± 0.8	0.1	−1.4	2	6

Note. [a] Cluster excluded from further analysis, due to $\Delta\mu_{\alpha\cos\delta}$ or $\Delta\mu_\delta > 5.0$ mas yr^{-1}.

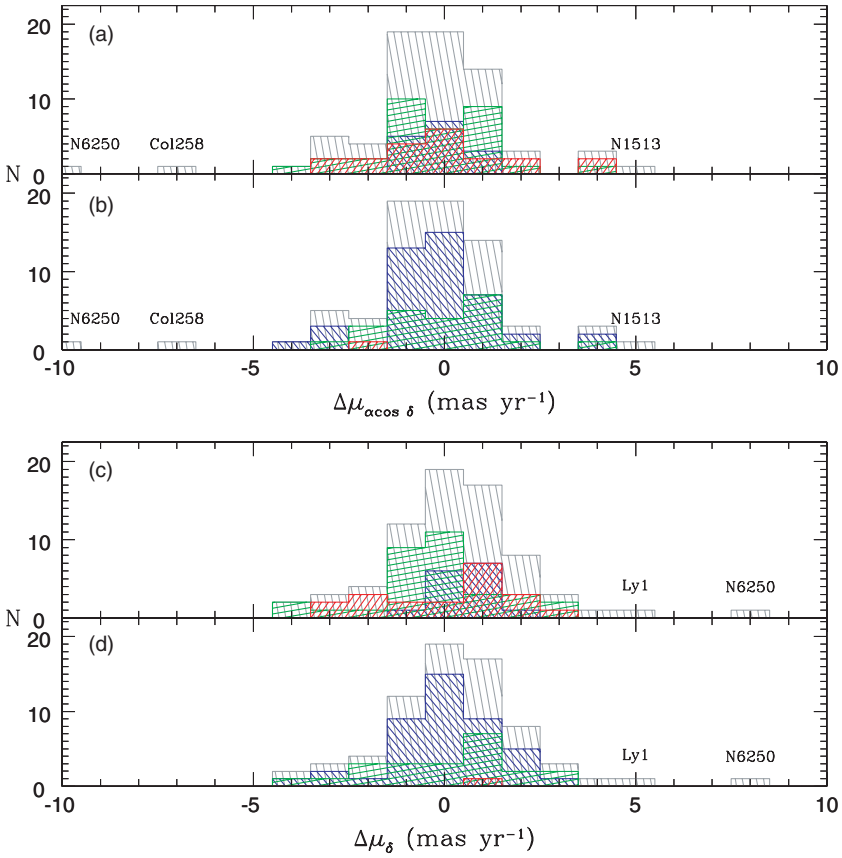

Figure 17. Comparison of the proper motions $\Delta\mu_{\alpha\cos\delta}$ and $\Delta\mu_\delta$ derived from our study to those of Dias et al. (2001, 2002a, Table 15). Histograms of $\Delta\mu$ showing that, besides the cases of Collinder 258, Lynga 1, and NGC 6250, all of our reliable measurements of the bulk RVs of the clusters are within 5 mas yr^{-1} of Dias et al. (2001, 2002a) study with the peak at $\Delta\mu_\alpha = 0$ mas yr^{-1} and $\Delta\mu_\delta = 0$ mas yr^{-1}. (a) $\Delta\mu_\alpha$ showing clusters having seven or more 3D members from our own analysis (blue histogram), while the green histogram denotes clusters with three to six 3D members, and the red histogram showing those clusters with less than three 3D members. (b) as (a) with histograms color-coded by membership from Dias et al., with the blue histogram having $\geqslant 20$ members, green 10–19 members, and red < 10 members. (c) $\Delta\mu_\delta$ with same color-coding as (a). (d) $\Delta\mu_\delta$ with same color-coding as (b).

each cluster, including, apparently, sufficient numbers of true members to get close to the correct proper motion. We show in Table 15 the numbers of Dias et al. member stars ($P_{\rm Dias} \geqslant 50\%$) that are confirmed to be members (Column 12) and how many we find to be unlikely members (Column 13) based on the addition of our RV analysis. On average, we find *half* of the Dias et al. "member" stars to be non-members when we account for the RVs. This suggests that use of proper motion data of the quality of *Tycho-2* alone may be insufficient to determine reliable cluster memberships, though, when averaged over many multiple stars and applying the 3σ rejection of outlier proper motions adopted by Dias et al., these proper motions are useful for deriving the cluster bulk proper motion. The Dias et al. membership inaccuracies are likely lessened for closer clusters (e.g., $d < 2$ kpc) which have more bright *Tycho-2* stars. Using the subsamples from Figure 17, we see that when both samples have a lot of "members" there is convergence to a common proper motion, as expected. We also see that as the sample sizes decrease the measured proper motion differences grow. It is clear that, at least in our case, when we have too few stars we may have trouble "finding" the true cluster members (e.g., as in the examples of NGC 1513 and NGC 7654). However, as both our

and the Dias et al. also studies drop to a few stars per clusters, it is difficult to determine which study is correct. We argue that given our more restrictive 3D membership criteria that ours is superior, though further study will be needed to confirm this assertion. Thus, while *Tycho-2* has the best currently available astrometric data, more strict RV discrimination such as we provide can substantially improve the application of these data for determining cluster motions, given a sufficient number of RV members.

7. SUMMARY

We have derived high-precision (typically < 3 km s^{-1} uncertainties) radial velocities for 3436 stars in the fields of 71 open clusters within 3 kpc of the Sun. This represents the largest sample of clusters assembled thus far having uniformly determined, high-precision radial velocities. To extend this uniformity to the other velocity dimensions, our survey has focused primarily on obtaining spectra of stars having measured *Tycho-2* proper motions; however, our target list was appended with other stars in the cluster fields to expand the membership census for each cluster. We have jointly applied three criteria—spatial position, radial velocity, and proper motion (in two dimensions)—to derive high-quality cluster membership probabilities for the samples stars. In at least half of our clusters we have found at least three stars in the field that are reliable members of the cluster using all of these criteria.

Using these member lists, we have averaged the RVs and the *Tycho-2* proper motions to derive mean space velocities for each cluster. With few exceptions, our mean cluster RVs are close to those previously derived for the several dozen clusters that have been surveyed by other groups. A comparison of our mean cluster proper motions with those by Dias et al. (2001, 2002a)—who also relied on *Tycho-2* proper motions—shows that both data sets are in general agreement, though our results should be more reliable given our more stringent assessment of cluster membership (i.e., we add high quality RVs to the proper motion criteria used by Dias et al.). We find that typically a large fraction of the Dias et al. stars in each cluster field do not meet our most restrictive, joint membership criteria. In a few cases with discrepant proper motion results compared to those derived by Dias et al. we find that the differences may be due to a critically small numbers of stars surviving our 3D "membership" criteria; i.e. in some of these cases (namely Collinder 258, Lynga 1, NGC 1513, NGC 6250, and NGC 7654) it is likely that our results, based on only one or two stars, might be wrong due to the improper identification of cluster members. Nevertheless, our data provide reliable 3D space motions for 66 open clusters.

In most cluster fields we have explored, our membership analysis provides valuable new benchmarks for improved isochrone fitting of the cluster CMDs, which is useful for estimating ages, distances, metallicities, and/or reddenings to these systems. The resulting distances and metallicities will allow a new attempt at measuring the Galactic metallicity gradient with these clusters. With improved distances and more reliable space velocities, the orbits of the clusters can be derived under an assumed Galactic potential and solar Galactocentric distance. Alternatively, these space velocities can be used as tracers of the local velocity field and be used to investigate the Galactic rotation curve with a set of objects having velocity independent distances and uniformly derived, quality space velocities. We intend to address these science issues in future contributions in this series.

Finally, our census of reliable cluster members provides a primary target list for future efforts to explore these open clusters with either high-resolution spectroscopy or high-precision astrometry, like that expected from *SIM PlanetQuest*.

We are grateful to W. Butler Burton for useful conversations and Ricardo Muñoz for discussions and assistance with the WIYN observations. We thank the anonymous referee for suggestions that helped the presentation of the paper. We would also like to thank the National Optical Astronomy Observatories (NOAO) for granting this Ph.D. dissertation project long-term observing status. We acknowledge travel support for PMF from NOAO. This project was supported by the *SIM PlanetQuest* key project *Taking Measure of the Milky Way* under NASA/JPL contract 1228235. We also acknowledge funding from NSF grant AST-0307851, a David and Lucile Packard Foundation Fellowship to SRM during the early stages of this project, and the F.H. Levinson Fund of the Peninsula Community Foundation. Additionally, PMF was supported by an NSF Astronomy and Astrophysics Postdoctoral Fellowship under award AST-0602221, the NASA Graduate Student Researchers Program, a University of Virginia Faculty Senate Dissertation-Year Fellowship, and grants from the Virginia Space Grant Consortium. The *Tycho-2* catalog is based on observations of the ESA *Hipparcos* satellite. This research has made use of the USNOFS Image and Catalogue Archive operated by the United States Naval Observatory, Flagstaff Station (http://www.nofs.navy.mil/data/fchpix/). The results presented in this publication also make use of data from the Two Micron All Sky Survey (2MASS), which is a joint project of the University of Massachusetts and the Infrared Processing and Analysis Center (IPAC), funded by the National Aeronautics and Space Administration and the National Science Foundation.

REFERENCES

Balaguer-Núñez, L., Galadí-Enríquez, D., & Jordi, C. 2007, A&A, 470, 585
Bastian, U., Röser, S., Yagudin, L. I., Nesterov, V. V., Polozhentsev, D. D., Potter, Kh. I., Wielen, R., & Yatskiv, Ya. S. 1993, in PPM star catalogue, Vols III & IV, (Heidelberg: Spektrum Akademischer)
Baumgardt, H., Dettbarn, C., & Wielen, R. 2000, A&AS, 146, 251
Becker, W., Svolopoulos, S. N., & Fang, C. 1976, in Kataloge photographischer und photoelektrischer Helligkeiten von 25 galaktischen Sternhaufen im *RGU*- und U_cBV-system, (Basel: Univ. Basel)
Bozkert, S. 1974, RevMexAA, 1, 89
Cannon, R. D. 1970, MNRAS, 150, 111
Carraro, G. 1999, in Galaxy Evolution: Connecting the Distant Universe with the Local Fossil Record Proc. of Colloquium 1998 September 21–25, ed. M. Spite (Berlin: Springer), 283 (reprinted from ApSS, 265, 1)
Chaboyer, B., Green, E. M., & Liebert, J. 1999, AJ, 117, 1360
Claria, J. J., & Mermilliod, J.-C. 1992, A&AS, 95, 429
Claria, J. J., Mermilliod, J.-C., & Piatti, A. E. 1999, A&AS, 134, 301
Claria, J. J., Mermilliod, J.-C., Piatti, A. E., Lapasset, E., & Mermilliod, J.-C. 2003, A&A, 399, 543
Clayton, G. C., & Fitzpatrick, E. L. 1987, AJ, 93, 157
Dias, W. S., Alessi, B. S., Moitinho, A., Lépine, J. R. D., & Alessi, B. S. 2002b, A&A, 389, 8718
Dias, W. S., Assafin, M., Florio, V., Alessi, B. S., & Libero, V. 2006, A&A, 446, 949
Dias, W. S., Lépine, J. R. D., & Alessi, B. S. 2001, A&A, 376, 441
Dias, W. S., Lépine, J. R. D., & Alessi, B. S. 2002a, A&A, 388, 168
Dutra, C. M., & Bica, E. 2000, A&A, 359, 347
Eggen, O. J., & Sandage, A. R. 1964, ApJ, 140, 130
Fan, et al. 1996, AJ, 112, 628
Fekel, F. C. 1999, in ASP Conf. Ser. 185, Precise Stellar Radial Velocities, ed. J. B. Hearnshaw, & C. D. Scarfe (Provo, UT: ASP)
Fich, M., Blitz, L., & Stark, A. A. 1989, ApJ, 342, 272
Forbes, D., English, D., De Robertis, M. M., & Dawson, P. C. 1992, AJ, 103, 916
Friel, E. D. 1995, ARA&A, 33, 381
Friel, E. D., & Janes, K. A. 1993, A&A, 267, 75
Frinchaboy, P. M. 2006a, Ph.D. Thesis, Univ. Virginia

Frinchaboy, P. M. 2006b, in ESO/Springer Conf. Proc., Globular Clusters—Guides to Galaxies, ed. T. Richtler, & S. Larsen, in press, arXiv astro-ph/0604133
Galadí-Enríquez, D., Jordi, C., & Trullols, E. 1998, A&A, 337, 125
Girard, T. M., Grundy, W. M., Lopez, C. E., & van Altena, W. F. 1989, AJ, 98, 227
Glushkova, E. V., Zabolotskikh, M. V., Rastorguev, A. S., Uglova, I. M., Fedorova, A. A., & Volchkov, A. A. 1996, AZh, 23, 850
Glushkova, E. V., Dambis, A. K., Mel'nik, A. M., & Rastorguev, A. S. 1998, A&A, 329, 514
Gonzalez, J. F., & Lapasset, E. 2001, AJ, 121, 2657
Grenier, S., Burnage, R., Faraggiana, R., Gerbaldi, M., Delmas, F., Gmez, A. E., Sabas, V., & Sharif, L. 1999, A&AS, 135, 503
Gulyaev, A. P., & Nesterov, V. V. 1992, O Chetyrekhmillionnom kataloge zvezd (On the Four-Million Star Catalogue), (Moscow: Izd. Mos. Gos. Univ.)
Hand, D. J. 1982, Kernel Discriminant Analysis, (Chichester: Research Studies Press)
Hassan, S. M. 1976, A&AS, 26, 13
Hron, J. 1987, A&A, 176, 34.
Janes, K. A., & Adler, D. 1982, ApJS, 49, 425
Jeffries, R. D., James, D. J., & Thurston, M. R. 1998, MNRAS, 300, 550
Kharchenko, N. V., Piskunov, A. E., Röser, S., Schilbach, E., & Scholz, R.-D. 2005, A&A, 438, 1163
Koester, D., & Reimers, D. 1996, A&A, 313, 810
Kopff, E. 1943, Astron. Nachr., 274, No 2
Lindoff, U. 1972, A&AS, 7, 133
Liu, T., Janes, K. A., & Bania, T. M. 1989, AJ, 98, 626
Loktin, A. V., & Beshenov, G. V. 2003, AZh, 80, 8
Lynga, G., & Palous, J. 1987, A&A, 188, 35
Maeder, A., & Mermilliod, J. C. 1981, A&A, 93, 136
Mathieu, R. D., Latham, D. W., Griffin, R. F., & Gunn, J. E. 1986, AJ, 92, 1100
Meibom, S., Andersen, J., & Nordström, B. 2002, A&A, 386, 187
Mermilliod, J.-C. 1995, in Information and On-Line Data in Astronomy, ed. D. Egret, & M. A. Albrecht (Dordrecht: Kluwer), 127–138
Mermilliod, J.-C., Andersen, J., Nordstroem, B., & Mayor, M. 1995, A&A, 299, 53
Mermilliod, J.-C., Huestamendia, G., del Rio, G., & Mayor, M. 1996, A&A, 307, 87
Mermilliod, J.-C., & Mayor, M. 1989, A&A, 219, 125
Mermilliod, J.-C., & Mayor, M. 1990, A&A, 237, 61
Mermilliod, J.-C., Mayor, M., & Burki, G. 1987, A&AS, 70, 389
Meynet, G., Mermilliod, J.-C., & Maeder, A. 1993, A&AS, 98, 477
Montgomery, K. A., Marschall, L. A., & Janes, K. A. 1993, AJ, 106, 181
Pesch, P. 1961, ApJ, 134, 602
Phelps, R. L. 1997, ApJ, 483, 826
Phelps, R. L., Janes, K. A., & Montgomery, K. A. 1994, AJ, 107, 1079
Prada Moroni, P. G., & Straniero, O. 2002, ApJ, 581, 585
Prichet, C. J., & Glaspey, J. W. 1991, ApJ, 373, 105
Pryor, T., & Meylan, G. 1993, in ASP Conf. Ser. 50, Structure and Dynamics of Globular Clusters, ed. Meylan, & Djorgovski (San Francisco, CA: ASP), 357
Robichon, N., Arenou, F., Mermilliod, J.-C., & Turon, C. 1999, A&A, 345, 471
Röser, S., Bastian, U., & Kuzmin, A. 1994, A&AS, 105, 301
Röser, S., & Bastian, U. 1991, in PPM star catalogue, Vols I & II, (Heidelberg: Spektrum Akademischer Verlag)
Salasnich, B., Girardi, L., Weiss, A., & Chiosi, C. 2000, A&A, 361, 1023
Sandage, A. 1957, ApJ, 125, 435
Sanders, W. L. 1977, A&AS, 27, 89
Schlegel, D. J., Finkbeiner, D. P., & Davis, M. 1998, ApJ, 500, 525
Scott, J. E., Friel, E. D., & Janes, K. A. 1995, AJ, 109, 1706
Skrutskie, M. F., et al. 2006, AJ, 131, 1163
Spitzer, L., & Schwarzschild, M. 1951, ApJ, 114, 407
Spitzer, L., & Schwarzschild, M. 1953, ApJ, 118, 106
Terndrup, D. M., Pinsonneault, M., Jeffries, R. D., Ford, A., Stauffer, J. R., & Sills, A. 2002, ApJ, 576, 950
Tonry, J., & Davis, M. 1979, AJ, 84, 1511
Trumpler, R. J. 1930a, Lick Observatory Bulletin, 14, 154
Trumpler, R. J. 1930b, PASP, 42, 214
Twarog, B. A. 1980, ApJ, 242, 242
Twarog, B. A., & Anthony-Twarog, B. J. 1989, AJ, 97, 759
Twarog, B. A., Ashman, K. M., & Anthony-Twarog, B. J. 1997, AJ, 114, 2556
Valitova, A. M., Rastorgouev, A. S., Sementsov, V. N., & Tokovinin, A. A. 1990, PAZh, 16, 699
Vogt, S. S., Mateo, M., Olszewski, E. W., & Keane, M. J. 1995, AJ, 109, 151
van Zeipel, H., & Lindgren, J. 1921, Kungl. Sven. Vet. Handl. 61 No 15
Volchkov, A. A., Kuz'min, A. V., & Nesterov, V. V. 1992, in O Chetyrekhmillionnom Kataloge Zvezd (On the Four-Million Star Catalog), ed. A. P. Gulyaev, & V. V. Nesterov (Moscow: Izd. MGU), 67
Zacharias, N., et al. 2004, AJ, 127, 3043